

Osmium Catalysts for Acceptorless and Base-Free Dehydrogenation of Alcohols and Amines: Unusual Coordination Modes of a BPI Anion

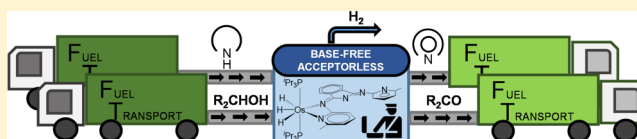
María L. Buil,[†] Miguel A. Esteruelas,^{*,†,‡} M. Pilar Gay,[†] Mar Gómez-Gallego,[‡] Antonio I. Nicasio,[†] Enrique Oñate,[†] Alicia Santiago,[‡] and Miguel A. Sierra^{*,‡}

[†]Departamento de Química Inorgánica, Instituto de Síntesis Química y Catálisis Homogénea (ISQCH), Centro de Innovación en Química Avanzada (ORFEO-CINQA), Universidad de Zaragoza-CSIC, 50009 Zaragoza, Spain

[‡]Departamento de Química Orgánica I, Facultad de CC. Químicas, Centro de Innovación en Química Avanzada (ORFEO-CINQA), Universidad Complutense de Madrid, 28040 Madrid, Spain

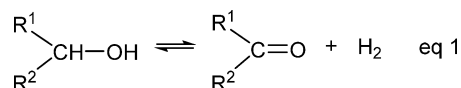
Supporting Information

ABSTRACT: A novel type of catalyst precursors for the dehydrogenation of hydrogen carriers based on organic liquids has been discovered. Complexes $\text{OsH}_6(\text{P}^i\text{Pr}_3)_2$ (**1**) and $\text{OsH}(\text{OH})(\text{CO})(\text{P}^i\text{Pr}_3)_2$ (**2**) react with 1,3-bis(6'-methyl-2'-pyridylimino)isoindoline (HBMePI) to give $\text{OsH}_3\{\kappa^2\text{-N}_{\text{py}},\text{N}_{\text{imine}}\text{-(BMePI)}\}(\text{P}^i\text{Pr}_3)_2$ (**3**) and $\text{OsH}\{\kappa^2\text{-N}_{\text{py}},\text{N}_{\text{imine}}\text{-(BMePI)}\}(\text{CO})(\text{P}^i\text{Pr}_3)_2$ (**4**). The unprecedented $\kappa^2\text{-N}_{\text{py}},\text{N}_{\text{imine}}$ coordination mode of BMePI is thermodynamically preferred with Os(IV) and Os(II) metal fragments and allows for preparation of BMePI-based dinuclear metal cations. Treatment of $\text{OsH}_2\text{Cl}_2(\text{P}^i\text{Pr}_3)_2$ (**5**) with 0.5 equiv of HBMePI in the presence of KO^tBu affords the chloride salt of the bis(osmium(IV)) dinuclear cation $[\{\text{OsH}_3(\text{P}^i\text{Pr}_3)_2\}_2\{\mu\text{-(}\kappa^2\text{-N}_{\text{py}},\text{N}_{\text{imine}}\text{)}_2\text{-BMePI}\}]^+$ (**6**). Related homoleptic bis(osmium(II)) complexes have been also synthesized. Complex **4** reacts with the bis(solvento) $[\text{OsH}(\text{CO})\{\kappa^1\text{-O-}[\text{OCMe}_2]_2\}(\text{P}^i\text{Pr}_3)_2]\text{BF}_4$ to give $[\{\text{OsH}(\text{CO})\text{-(P}^i\text{Pr}_3)_2\}_2\{\mu\text{-(}\kappa^2\text{-N}_{\text{py}},\text{N}_{\text{imine}}\text{)}_2\text{-BMePI}\}]\text{BF}_4$ (**7**), whereas the addition of 0.5 equiv of HBMePI to $\{\text{OsCl}(\eta^6\text{-C}_6\text{H}_6)\}_2(\mu\text{-Cl})_2$ (**8**) affords $[\{\text{OsCl}(\eta^6\text{-C}_6\text{H}_6)\}_2\{\mu\text{-(}\kappa^2\text{-N}_{\text{py}},\text{N}_{\text{imine}}\text{)}_2\text{-BMePI}\}]\text{Cl}$ (**9**). The reactions of **4** with **8** and $\{\text{OsCl}(\eta^6\text{-p-cymene})\}_2(\mu\text{-Cl})_2$ (**10**) lead to the heteroleptic cations $[(\text{P}^i\text{Pr}_3)_2(\text{CO})\text{Hos}\{\mu\text{-(}\kappa^2\text{-N}_{\text{py}},\text{N}_{\text{imine}}\text{)}_2\text{-BMePI}\}\text{OsCl}(\eta^6\text{-arene})]^+$ (arene = C_6H_6 (**11**), *p*-cymene (**12**)). The electronic structure and electrochemical properties of the dinuclear complexes were also studied. Complexes **3** and **4** are efficient catalyst precursors for the acceptorless and base-free dehydrogenation of secondary and primary alcohols and cyclic and lineal amines. The primary alcohols afford aldehydes. The amount of H_2 released per gram of heterocycle depends upon the presence of a methyl group adjacent to the nitrogen atom, the position of the nitrogen atom in the heterocycle, and the size of the heterocycle.



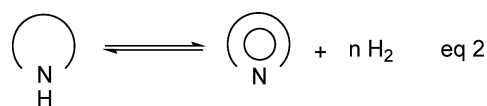
INTRODUCTION

Catalytic acceptorless alcohol dehydrogenation (eq 1) is a reaction of great interest in connection with the hydrogen production from biomass and the hydrogen storage/transport in organic liquids. The process is an oxidant-free atom-economical approach for the oxidation of alcohols to carbonyl compounds,¹ and although the reaction is generally endothermic at room temperature, the equilibrium can be driven by removal of H_2 .



The most attractive hydrogen carriers based on organic liquids are the cycloalkanes, as they have a relatively high hydrogen content and also can be transported through the liquid-fuel infrastructures. Nevertheless, their large enthalpy of dehydrogenation is a drawback for practical applications. The introduction of a heteroatom into the ring system significantly decreases the enthalpy of dehydrogenation. As a consequence, the metal-promoted acceptorless dehydrogenation of cyclic

amines is a reaction which is also waking a great interest (eq 2).²



Platinum group metals form the most efficient homogeneous catalysts for these reactions and therefore are highly relevant from an environmental point of view, in particular those of ruthenium^{3,4} and iridium,^{5,6} although nonprecious metals have also given rise to interesting catalysts.^{7,8} High temperatures and strong basic media are often employed to promote the catalysis.^{3e,k,m,o,5a,b,7a,d,f} An alternative that avoids the use of additives involves catalysts bearing ligands with heteroatoms having sufficiently basic free electron pairs.^{1e,2a}

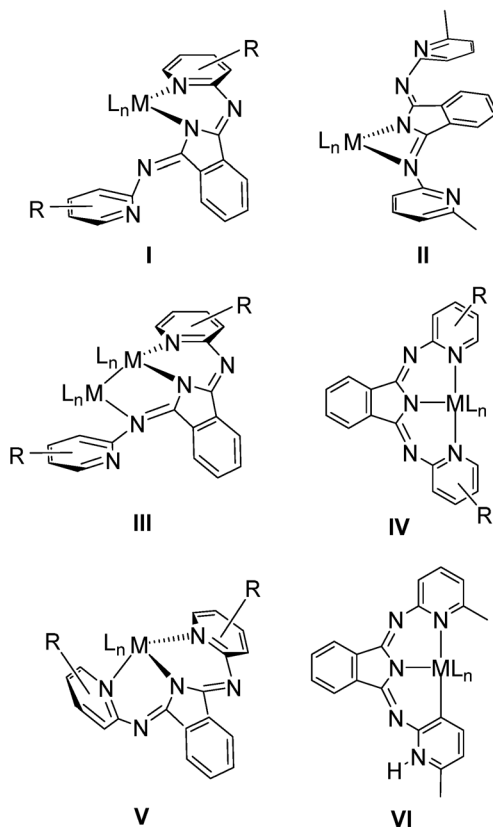
1,3-Bis(2-pyridylimino)isoindolates (BPIs) are a class of monoanionic ligands with five basic nitrogen atoms,⁹ which

Received: December 22, 2017

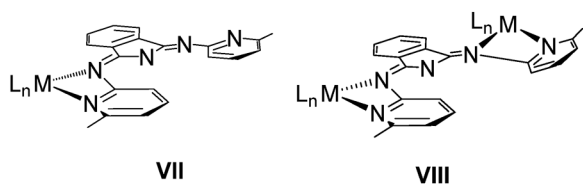
show $\kappa^2\text{-N}_{\text{py}}\text{N}_{\text{iso}}$, $\kappa^2\text{-N}_{\text{iso}}\text{N}_{\text{imine}}$,¹⁰ $\kappa^3\text{-(N}_{\text{py}}\text{N}_{\text{iso}}\text{N}_{\text{imine}}\text{)-bridge}$,¹¹ $\kappa^3\text{-(N}_{\text{py}}\text{N}_{\text{iso}}\text{N}_{\text{py}}\text{)-mer}$,¹² and $\kappa^3\text{-(N}_{\text{py}}\text{N}_{\text{iso}}\text{N}_{\text{py}}\text{)-fac}$ ¹⁰ coordination modes (I to V in Chart 1), leaving free at least two basic

Chart 1. BPI Coordination Modes

Previous Work



This Work



heteroatoms. Hence, BPIs could be able to stabilize catalysts for the acceptorless dehydrogenation of alcohols and amines avoiding the use of strong basic media.^{3b,j}

Osmium is the less used platinum group metal in catalysis, with the notable exception of the Sharpless dihydroxylation and reactions akin.¹³ However, this metal appears to be a promising alternative for reactions related to hydrogen economy.¹⁴ For instance, in 2011, Baratta and co-workers reported that diamine-diphosphine osmium complexes promote the acceptorless dehydrogenation of alcohols to ketones, in basic medium, with activities comparable to those of their ruthenium counterparts.¹⁵ Also, we have recently demonstrated that the trihydride-acetylacetonate complex $\text{OsH}_3(\text{acac})(\text{P}^i\text{Pr}_3)_2$ catalyzes the acceptorless dehydrogenation of cyclic amines.¹⁶

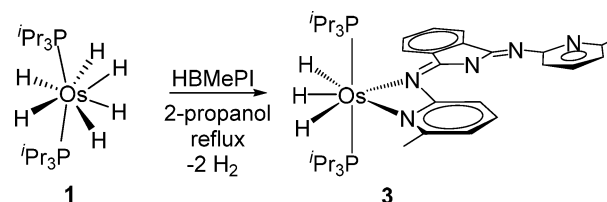
In the search for osmium catalysts for the base-free and acceptorless dehydrogenation of alcohols and cyclic amines, we have studied the reactions of complexes $\text{OsH}_6(\text{P}^i\text{Pr}_3)_2$ (1) and

$\text{OsH}(\text{OH})(\text{CO})(\text{P}^i\text{Pr}_3)_2$ (2) with 1,3-bis(6'-methyl-2'-pyridylimino)isoindoline (HBMePI). This molecule is a sterically demanding version of HBPI,¹⁷ which allows a $\kappa^3\text{-(N}_{\text{py}}\text{N}_{\text{iso}}\text{C}_{\text{Hpy}}\text{)-mer}$ coordination of the BMePI anion¹⁸ (VI in Chart 1), in agreement with other α -substituted *N*-heterocycles.¹⁹ During this study, we have discovered an unprecedented $\kappa^2\text{-N}_{\text{py}}\text{N}_{\text{imine}}$ coordination mode of a BPI anion (VII in Chart 1). This paper reports (i) the unprecedented $\kappa^2\text{-N}_{\text{py}}\text{N}_{\text{imine}}$ coordination of the BMePI anion, (ii) a thermodynamic perspective of its existence, (iii) the $\mu\text{-(}\kappa^2\text{-N}_{\text{py}}\text{N}_{\text{imine}}\text{)}_2$ coordination of BMePI (VIII in Chart 1), and (iv) the catalytic activity of the $\text{Os}(\kappa^2\text{-N}_{\text{py}}\text{N}_{\text{imine}})$ complexes in the acceptorless and base-free dehydrogenation of alcohols and amines.

RESULTS AND DISCUSSION

$\kappa^2\text{-N}_{\text{py}}\text{N}_{\text{imine}}$ Complexes. Polyhydrides of platinum group metals are a class of transition-metal compounds, which have the ability of activating σ -bonds.²⁰ In particular, the d^2 -hexahydride complex 1 has proved to promote the rupture of C–H,²¹ C–C,²² C–N,²³ O–H,²⁴ and N–H²⁵ bonds. In agreement with this, the treatment of 2-propanol solutions of this polyhydride with 1.0 equiv of HBMePI, under reflux, for 6 h leads to the trihydride-osmium(IV) derivative $\text{OsH}_3\{\kappa^2\text{-N}_{\text{py}}\text{N}_{\text{imine}}\text{-(BMePI)}\}(\text{P}^i\text{Pr}_3)_2$, as a result of the deprotonation of the polycycle, by action of a hydride ligand, and the coordination of a pyridyl group and its adjacent imine function of the resulting anion. Complex 3 was isolated as a red solid in 67% yield (Scheme 1).

Scheme 1. Formation of 3



The novel $\kappa^2\text{-N}_{\text{py}}\text{N}_{\text{imine}}$ coordination of the BMePI anion to the $[\text{OsH}_3(\text{P}^i\text{Pr}_3)_2]^+$ metal fragment was confirmed by means of the X-ray diffraction analysis structure of 3. Figure 1 shows a view of the molecule. The coordination geometry around the osmium atom can be described as a distorted pentagonal bipyramid with axial phosphines ($\text{P}(1)\text{--Os--P}(2) = 168.07(8)^\circ$). The metal coordination sphere is completed by the hydride ligands separated by $1.63(9)$ ($\text{H}(01)$ and $\text{H}(02)$) and $1.61(9)$ ($\text{H}(02)$ and $\text{H}(03)$) Å and the pyridine $\text{N}(1)$ and imine $\text{N}(2)$ atoms of the chelate BMePI anion, which acts with a $\text{N}(1)\text{--Os--N}(2)$ bite angle of $59.7(3)^\circ$. The osmium–pyridine bond length of $2.168(7)^\circ$ ($\text{Os--N}(1)$) is about 0.04 Å shorter than the osmium–imine distance of $2.207(7)$ ($\text{Os--N}(2)$) Å. The classical trihydride nature of the complex was confirmed by the DFT-optimized structure (B3LYP/def2-SVP) and the hydride resonances in the ^1H NMR spectrum. The DFT calculations yield separations between the hydrides of 1.574 and 1.573 Å, which agree well with those obtained from the X-ray diffraction analysis. The ^1H NMR spectrum, at 193 K, in dichloromethane- d_2 shows three high field signals centered at -10.68 , -12.15 , and -13.89 ppm corresponding to the inequivalent hydrides. As expected for equivalent phosphines, the $^{31}\text{P}\{^1\text{H}\}$ NMR spectrum displays a singlet at 20.1 ppm.

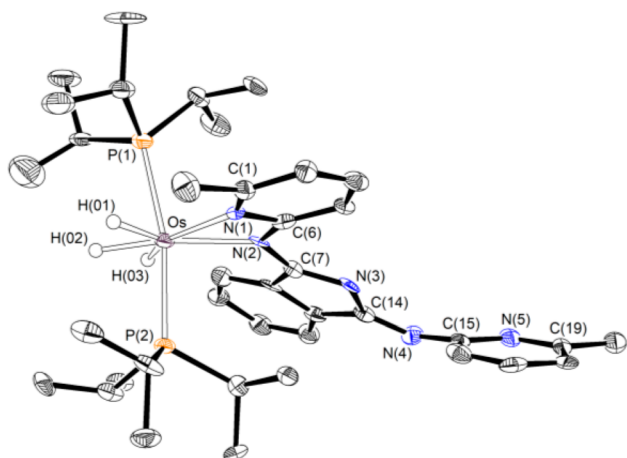
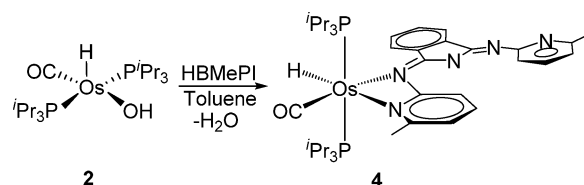


Figure 1. Molecular diagram of complex **3** (50% probability ellipsoids). All hydrogen atoms (except the hydrides) are omitted for clarity. Selected bond lengths (Å) and angles (deg): Os–N(1) = 2.168(7), Os–N(2) = 2.207(7), N(1)–C(6) = 1.341(11), N(2)–C(6) = 1.392(11), N(2)–C(7) = 1.339(11), N(3)–C(7) = 1.343(11), N(3)–C(14) = 1.378(10), N(4)–C(14) = 1.294(11), N(4)–C(15) = 1.391(11), P(1)–Os–P(2) = 168.07(8), N(1)–Os–N(2) = 59.7(3).

Gade and co-workers have reported cationic and neutral osmium-bis(triphenylphosphine) complexes containing a κ^3 -($N_{py}N_{iso}N_{py}$)-*mer* BPI ligand²⁶ and half-sandwich species with the polydentate anion coordinated κ^3 -($N_{py}N_{iso}N_{py}$)-*fac* or κ^2 - $N_{py}N_{iso}$.¹⁰ The difference in the oxidation state of the metal center, +2 in these compounds and +4 in **3**, prompted us to carry out the reaction between the hydroxide–osmium(II) complex **2** and HBMePI, in order to determine the influence of the oxidation state of the metal center in the coordination fashion of the BMePI anion. The hydroxide group in **2** should promote the deprotonation of the polycycle in the same way as the hydrides of **1**. In fact, the treatment of toluene solutions of **2** with 1.1 equiv of HBMePI, at room temperature, for 2 h produces the deprotonation of the polycycle. Interestingly, the resulting BMePI anion coordinates to the $[OsH(CO)(P^iPr_3)_2]^+$ metal fragment as in **3**, κ^2 - $N_{py}N_{imine}$, in spite of the +2 oxidation state of the metal center. This clearly indicates that the oxidation state of the metal center does not determine the mode of coordination of the BMePI ligand. The new osmium(II) complex $OsH\{\kappa^2-N_{py}N_{imine}-(BMePI)\}(CO)-(P^iPr_3)_2$ (**4**) was isolated as an orange solid in 60% yield (Scheme 2).

Scheme 2. Formation of **4**



Complex **4** was also characterized by X-ray diffraction analysis. The structure, which demonstrated the novel coordination of the BMePI anion again, has two chemically equivalent but crystallographically independent molecules in the asymmetric unit. Figure 2 shows one of them. The coordination geometry around the osmium atom can be rationalized as derived from a distorted octahedron with the

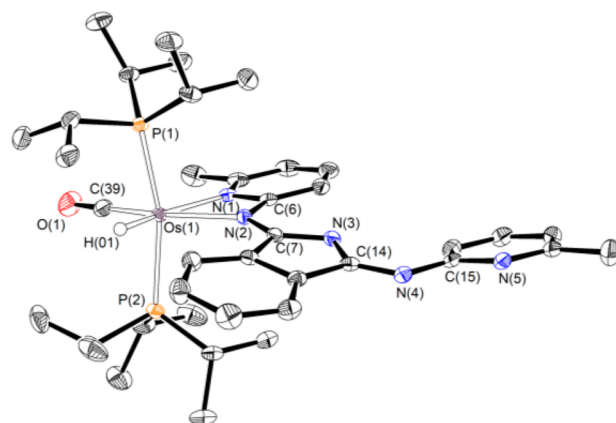


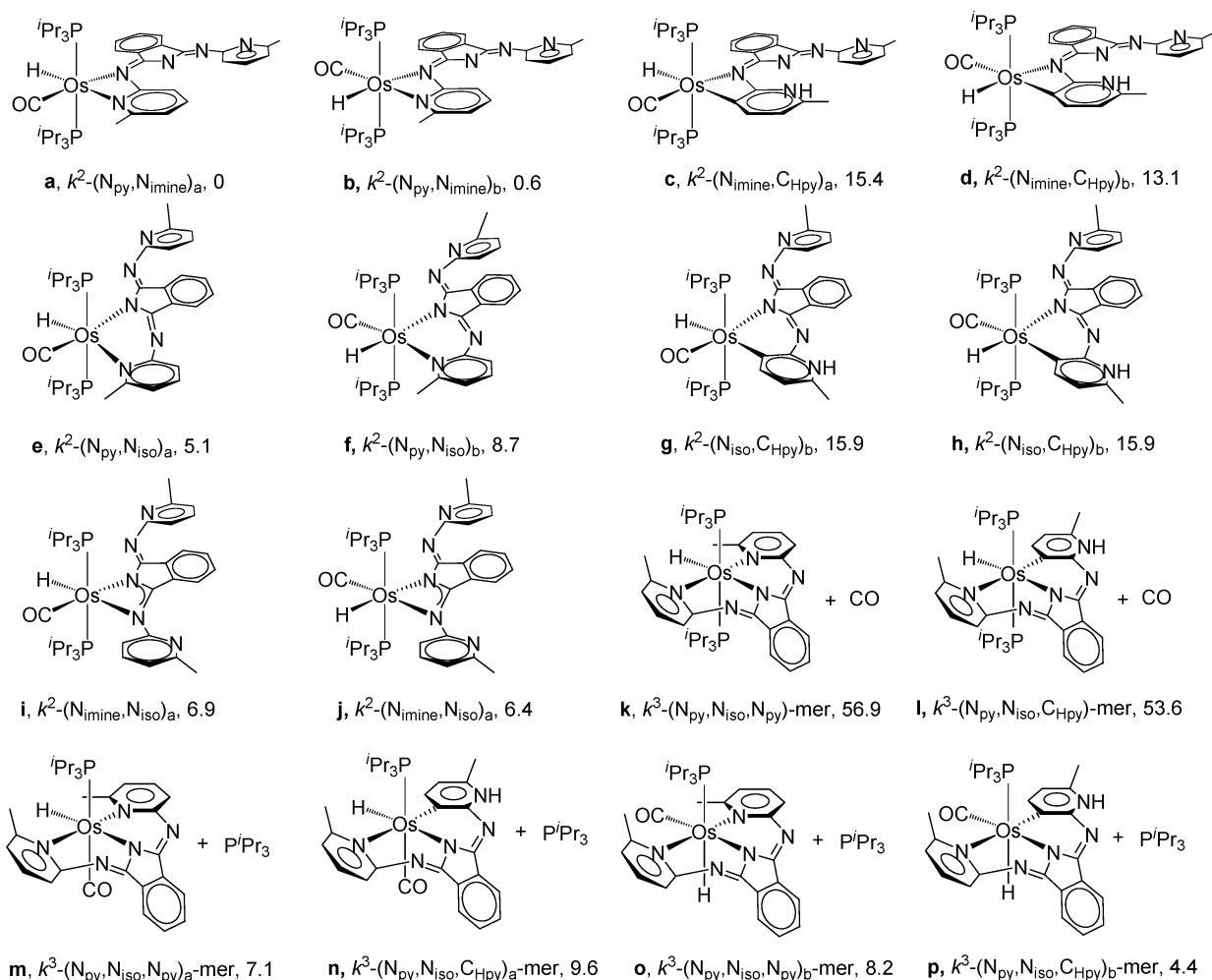
Figure 2. Molecular diagram of complex **4** (50% probability ellipsoids). All hydrogen atoms (except the hydride) are omitted for clarity. Selected bond lengths (Å) and angles (deg): Os(1)–N(1) = 2.175(4) and 2.173(4), Os(1)–N(2) = 2.229(4) and 2.230(4), N(2)–C(6) = 1.402(5) and 1.412(5), N(2)–C(7) = 1.329(5) and 1.326(5), N(3)–C(7) = 1.359(6) and 1.350(5), N(3)–C(14) = 1.387(5) and 1.380(5), N(4)–C(14) = 1.304(6) and 1.301(6), N(4)–C(15) = 1.403(6) and 1.403(6), P(1)–Os(1)–P(2) = 162.86(4) and 161.47(4), N(1)–Os(1)–N(2) = 60.30(13) and 60.44(13), H(01)–Os(1)–N(1) = 164.1(17) and 163.0(17), C(39)–Os(1)–N(2) = 165.29(17) and 164.51(18).

phosphines occupying *trans* positions (P(1)–Os(1)–P(2) = 162.86(4)° and 161.47(4)°). The perpendicular plane is formed by the chelate BMePI anion, which acts with N(1)–Os(1)–N(2) bite angles of 60.30(13)° and 60.44(13)°, the hydride disposed *trans* to the pyridine N(1) atom (H(01)–Os(1)–N(1) = 164.1(17)° and 163.0(17)°), and the carbonyl group located *trans* to the imine N(2) atom (C(39)–Os(1)–N(2) = 165.29(17)° and 164.51(18)°). The osmium–pyridine bond lengths of 2.175(4) and 2.173(4) (Os(1)–N(1)) Å, as well as the osmium–imine distances of 2.229(4) and 2.230(4) (Os(1)–N(2)) Å, are slightly longer than the respective parameters in **2**, which is consistent with the different oxidation states of the compounds. According to the presence of the hydride ligand, the ¹H NMR spectrum of **4**, in dichloromethane-*d*₂, at room temperature shows a triplet (²*J*_{H–P} = 20.3 Hz) at –14.00 ppm. The ³¹P{¹H} NMR spectrum contains a singlet at 19.5 ppm for the equivalent phosphines.

Perspective on the Formation of $Os\{\kappa^2-N_{py}N_{imine}-(BMePI)\}$ Complexes. To gain insight into why complexes **3** and **4** coordinate the BMePI ligand in a κ^2 - $N_{py}N_{imine}$ fashion, we calculated the energy of the optimized structures resulting from bending the metal fragment $[OsH(CO)(P^iPr_3)_2]^+$ to this anion in all possible forms. The free energy ΔG (kcal·mol^{–1}) was computed at the B3LYP/def2-SVP level, in toluene, at 298 K, and 1 atm. The results are summarized in Chart 2.

The κ^2 - $N_{py}N_{imine}$ coordination generates the most stable structures. Although for this coordination two isomers of similar stability are possible in the perpendicular plane to the P–Os–P direction, pyridine *trans* to H (a) and pyridine *trans* to CO (b), only the first of them is observed. This suggests that the formation of **4** (isomer a) is kinetically controlled and starts with the coordination of one of the pyridyl groups at the coordination vacancy of **2**, which lies *trans* to the hydride ligand. Thus, the adjacent imine N atom could displace the hydroxide ligand from the metal coordination sphere. The free OH[–] group should subsequently deprotonate the isoindoline. Once a is formed, the activation barrier for its isomerization

Chart 2. Optimized Structures and Energies Resulting from the Coordination of the BMePI Ligand to the Metal Fragment $[\text{OsH}(\text{CO})(\text{P}^i\text{Pr}_3)_2]^+$ in All Possible Options



into **b** appears to be too high. Isomer **a** is stable at least 24 h, in toluene, under reflux. This is consistent with the high octahedral Δ_o splitting of the $5d^6$ ions, which leads to low-spin configurations with a maximized ligand-field stabilization energy.²⁷ In spite of α -substituted pyridines having a poor coordination power and usually undergoing tautomerization to afford N-heterocycle carbenes with a N–H wingtip,¹⁹ here, the tautomerization is disadvantaged. Isomers **c** and **d** with $\kappa^2\text{-C}_{\text{Hpy}}, \text{N}_{\text{imine}}$ coordination are 15.4 and 13.1 kcal·mol^{−1} less stable than the respective $\kappa^2\text{-N}_{\text{py}}, \text{N}_{\text{imine}}$ derivatives.

Isomer **a** showing $\kappa^2\text{-N}_{\text{py}}, \text{N}_{\text{imine}}$ coordination is between 5 and 9 kcal·mol^{−1} more stable than the structures resulting from a $\kappa^2\text{-N}_{\text{py}}, \text{N}_{\text{iso}}$ binding to $[\text{OsH}(\text{CO})(\text{P}^i\text{Pr}_3)_2]^+$ (isomers **e** and **f**, respectively). The $\kappa^2\text{-N}_{\text{py}}, \text{N}_{\text{iso}}$ coordination has been observed in half-sandwich iridium(III) derivatives as an intermediate step in the formation of $\kappa^3\text{-(N}_{\text{py}}, \text{N}_{\text{iso}}, \text{N}_{\text{py}})\text{-fac}$ species and $\kappa^3\text{-(N}_{\text{py}}, \text{N}_{\text{iso}}, \text{C}_{\text{Hpy}})\text{-fac}$ derivatives containing a dianionic ligand resulting from the deprotonation of the free pyridyl group.¹⁰ Isomers **g** and **h** with $\kappa^2\text{-C}_{\text{Hpy}}, \text{N}_{\text{iso}}$ coordination remain being about 16 kcal·mol^{−1} less stable than the structure of the isolated isomer **a**, whereas the structures with coordination $\kappa^2\text{-N}_{\text{imine}}, \text{N}_{\text{iso}}$ (isomers **i** and **j**) lie about 7 kcal·mol^{−1} above the latter.

The terdentate coordination of the BMePI anion involves the donation of $6e^-$ from the ligand to the metal center. Because

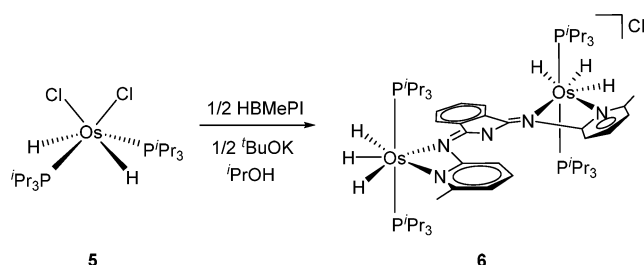
the latter in $[\text{OsH}(\text{CO})(\text{P}^i\text{Pr}_3)_2]^+$ possess $14e^-$, a $2e^-$ donor ligand (CO or P^iPr_3) must be released from the osmium coordination sphere in order to satisfy the 18-Electron Rule. The release of carbon monoxide produces a marked loss of stability. Thus, the resulting systems **k** and **l** lie between 53 and 57 kcal·mol^{−1}, respectively, above **a**, whereas the displacement of triisopropylphosphine generates systems **m–p**, which are only 4–10 kcal·mol^{−1} less stable than **a**. They have free energies similar to those of the derivatives with bidentate coordinations different from $\kappa^2\text{-N}_{\text{py}}, \text{N}_{\text{imine}}$. This agrees well with the strong backbonding ability of osmium.

$\mu\text{-(}\kappa^2\text{-N}_{\text{py}}, \text{N}_{\text{imine}})_2$ Complexes. In view of the high stability of the $\kappa^2\text{-N}_{\text{py}}, \text{N}_{\text{imine}}$ coordination, we asked ourselves if complexes **3** and **4** could be used as metalloligands to prepare dinuclear species and if the BMePI anion could act as a bridge with a double $\kappa^2\text{-N}_{\text{py}}, \text{N}_{\text{imine}}$ coordination. Indeed, homoleptic species with two osmium(IV) centers and homoleptic and heteroleptic derivatives with two osmium(II) centers, which contain a $\mu\text{-(}\kappa^2\text{-N}_{\text{py}}, \text{N}_{\text{imine}})_2$ bridge, can be synthesized employing strategies adapted to each particular case.

Treatment of the osmium(IV) complex $\text{OsH}_2\text{Cl}_2(\text{P}^i\text{Pr}_3)_2$ (**5**) with 0.5 equiv of HBMePI and 0.6 equiv of KO^tBu , in 2-propanol,²⁸ at room temperature, for 4 h affords the salt $[\{\text{OsH}_3(\text{P}^i\text{Pr}_3)_2\}_2\{\mu\text{-(}\kappa^2\text{-N}_{\text{py}}, \text{N}_{\text{imine}})_2\text{-BMePI}\}]\text{Cl}$ (**6**), containing a cation that can be formally described as the result of the

coordination of a $[\text{OsH}_3(\text{P}^i\text{Pr}_3)_2]^+$ metal fragment to the free chelate- $\text{N}_{\text{py}}\text{N}_{\text{imine}}$ moiety of **3**. This salt was isolated as a dark-purple solid in 49% yield (Scheme 3).

Scheme 3. Formation of **6**



The $\mu-(\kappa^2\text{-N}_{\text{py}}\text{N}_{\text{imine}})_2$ coordination of the BMePI anion in **6** was confirmed by X-ray diffraction analysis. Figure 3 shows a

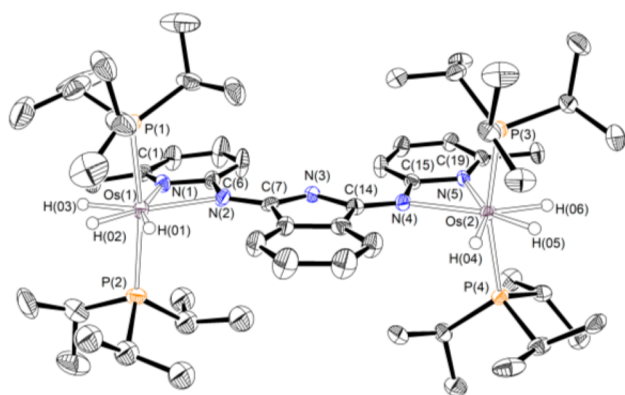


Figure 3. Molecular diagram of complex **6** (50% probability ellipsoids). All hydrogen atoms (except the hydrides) are omitted for clarity. Selected bond lengths (Å) and angles (deg): Os(1)–N(1) = 2.151(4), Os(2)–N(5) = 2.155(4) Å, Os(1)–N(2) = 2.208(4), Os(2)–N(4) = 2.219(4), N(2)–C(6) = 1.421(6), N(2)–C(7) = 1.323(6), N(3)–C(7) = 1.355(6), N(3)–C(14) = 1.358(6), N(4)–C(14) = 1.325(6), N(4)–C(15) = 1.406(6), P(1)–Os(1)–P(2) = 168.21(15)°, P(3)–Os(2)–P(4) = 164.21(4)°, N(1)–Os(1)–N(2) = 61.00(16)°, N(4)–Os(2)–N(5) = 60.88(15)°.

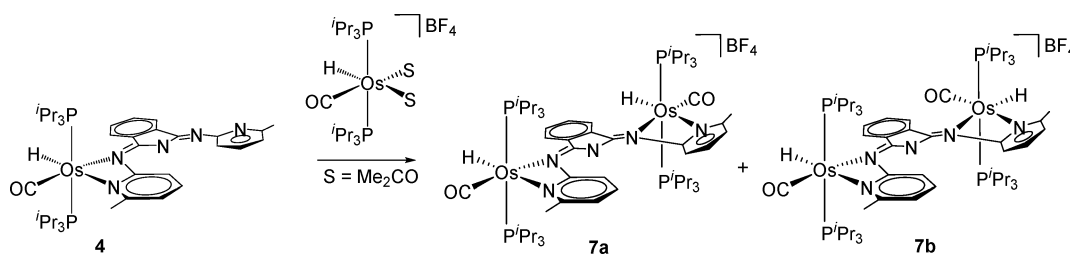
view of the cation of the salt, which is formed by two chemically equivalent $\text{OsH}_3(\kappa^2\text{-N}_{\text{py}}\text{N}_{\text{imine}})(\text{P}^i\text{Pr}_3)_2$ moieties connected to each other through an isoindoline linker. The coordination polyhedron around the osmium atoms resembles that of **3** with P(1)–Os(1)–P(2), P(3)–Os(2)–P(4), N(1)–Os(1)–N(2), and N(4)–Os(2)–N(5) angles of 168.21(15)°, 164.21(4)°, 61.00(16)°, and 60.88(15)°, respectively. The osmium–pyridine bond lengths of 2.151(4) (Os(1)–N(1)) and 2.155(4) (Os(2)–N(5)) Å, the osmium–imine distances of

2.208(4) (Os(1)–N(2)) and 2.219(4) (Os(2)–N(4)) Å, and the separations between the hydride ligands of 1.49(6) (H(01) and H(02)), 1.49(7) (H(02) and H(03)), 1.52(5) (H(04) and H(05)), and 1.65(5) (H(05) and H(06)) Å are also similar to the respective parameters of **3**. The classical trihydride nature of the OsH_3 units, which is notable considering the cationic nature of this species,^{20,29} was confirmed by the DFT-optimized structure (B3LYP/def2-SVP). In agreement with the X-ray diffraction structure, it displays separations between the hydride ligands of 1.571 (H(01) and H(02)), 1.583 (H(02) and H(03)), 1.559 (H(04) and H(05)), and 1.586 (H(05) and H(06)) Å. As expected for chemically equivalent $\text{OsH}_3(\text{P}^i\text{Pr}_3)_2$ moieties, which contain three inequivalent hydride ligands, the ^1H NMR spectrum, in dichloromethane- d_2 , at 193 K shows three high field signals at –10.78, –12.11, and –13.95 ppm. The $^{31}\text{P}\{^1\text{H}\}$ NMR spectrum displays a singlet at 20.9 ppm corresponding to the equivalent phosphines.

The coordination ability of the free chelate- $\text{N}_{\text{py}}\text{N}_{\text{imine}}$ moiety of $\text{Os}\{\kappa^2\text{-N}_{\text{py}}\text{N}_{\text{imine}}(\text{BMePI})\}$ -complexes is also demonstrated by the reaction summarized in Scheme 4. The free pyridine N(5) and imine N(4) atoms of **4** displace the coordinated acetone molecules of the bis(solvento) $[\text{OsH}(\text{CO})\{\kappa^1\text{-O}[\text{OCMe}_2]_2\}_2(\text{P}^i\text{Pr}_3)_2]\text{BF}_4$.³⁰ This species is asymmetrical in any plane containing the P–Os–P direction. So, at first glance, two coordination ways of the chelate- $\text{N}_{\text{py}}\text{N}_{\text{imine}}$ moiety are possible, pyridine *trans* to hydride and pyridine *trans* to carbonyl, as in isomers **a** and **b** of Chart 2. According to their similar stability, the displacement leads to $[\{\text{OsH}(\text{CO})-(\text{P}^i\text{Pr}_3)_2\}_2\{\mu-(\kappa^2\text{-N}_{\text{py}}\text{N}_{\text{imine}})_2\text{-BMePI}\}]\text{BF}_4$ (**7**), which is formed as the mixture of isomers **7a** and **7b** shown in Scheme 4. The mixture was isolated as a dark purple solid in 67% yield.

Figure 4 shows a view of **7a**. The structure proves that both $\text{OsH}(\text{CO})(\text{P}^i\text{Pr}_3)_2$ metal fragments coordinate to the chelate- $\text{N}_{\text{py}}\text{N}_{\text{imine}}$ units in the same manner, with the pyridine N(1) and N(5) atoms *trans* to the respective hydride ligand (N(1)–Os(1)–H(01) = 167(5)° and N(5)–Os(2)–H(02) = 165(4)°) and the imine N(2) and N(4) atoms *trans* to the respective carbonyl groups (N(2)–Os(1)–C(20) = 164.1(5)° and N(4)–Os(2)–C(21) = 165.3(5)°). Thus, the coordination polyhedron around each osmium atom is as in **4** with P(1)–Os(1)–P(2) and P(3)–Os(2)–P(4) angles of 162.08(12)° and 163.37(12)°, respectively. The osmium–pyridine bond lengths of 2.148(9) (Os(1)–N(1)) and 2.166(10) (Os(2)–N(5)) Å as well as the osmium–imine distances of 2.243(9) (Os(1)–N(2)) and 2.217(8) (Os(2)–N(4)) Å are statistically identical to the corresponding parameters of **4**. The equivalence of the metal fragments is also revealed by the ^1H and $^{31}\text{P}\{^1\text{H}\}$ NMR spectra, in dichloromethane- d_2 , at room temperature. Thus, the ^1H NMR spectrum shows a hydride resonance at –14.45, which appears as a triplet with a H–P coupling

Scheme 4. Formation of the Mixture of Isomers **7a** and **7b**



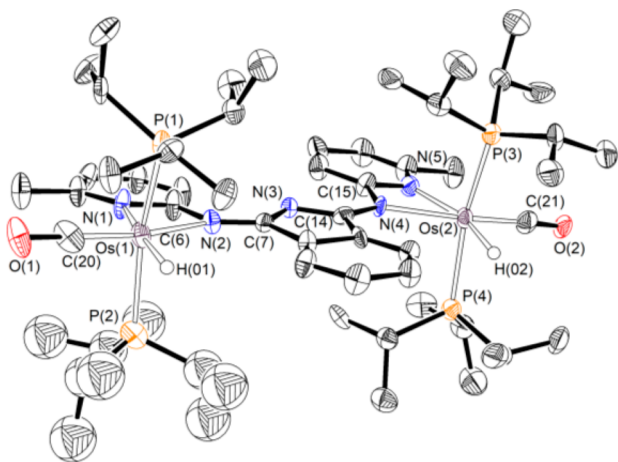


Figure 4. Molecular diagram of complex **7a** (50% probability ellipsoids). All hydrogen atoms (except the hydrides) are omitted for clarity. Selected bond lengths (Å) and angles (deg): Os(1)–N(1) = 2.148(9), Os(2)–N(5) = 2.166(10), Os(1)–N(2) = 2.243(9), Os(2)–N(4) = 2.217(8), N(2)–C(6) = 1.407(14), N(2)–C(7) = 1.279(13), N(3)–C(7) = 1.351(14), N(3)–C(14) = 1.346(14), N(4)–C(14) = 1.364(13), N(4)–C(15) = 1.387(14), N(1)–Os(1)–H(01) = 167(5), N(5)–Os(2)–H(02) = 165(4), N(2)–Os(1)–C(20) = 164.1(5), N(4)–Os(2)–C(21) = 165.3(5), P(1)–Os(1)–P(2) = 162.08(12), P(3)–Os(2)–P(4) = 163.37(12).

constant of 20.0 Hz, whereas the $^{31}\text{P}\{^1\text{H}\}$ NMR spectrum exhibits a singlet at 20.2 ppm for the four phosphine ligands.

Complex **7b** has been also characterized by X-ray diffraction analysis. **Figure 5** shows a view of the cation. Although both metal centers display an octahedral environment with *trans* phosphines (P(1)–Os(1)–P(2) = 163.12(4)° and P(3)–Os(2)–P(4) = 164.51(4)°), in this case, only one of the coordination polyhedral resembles that of **4** with the hydride ligand *trans* to the pyridine (N(1)–Os(1)–H(01) =

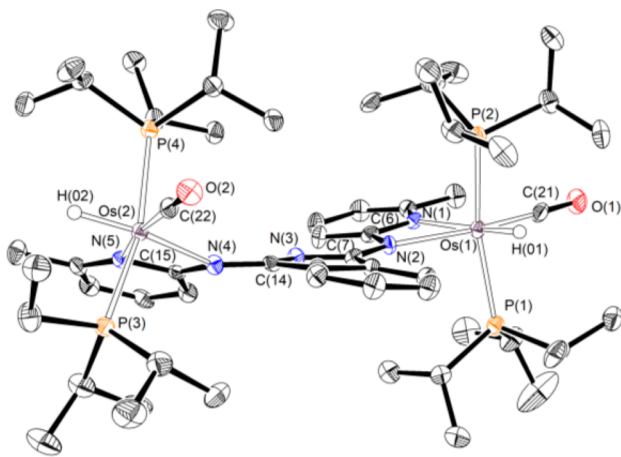
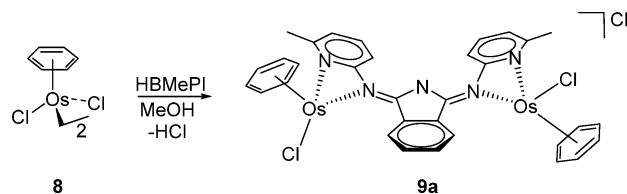


Figure 5. Molecular diagram of complex **7b** (50% probability ellipsoids). All hydrogen atoms (except the hydrides) are omitted for clarity. Selected bond lengths (Å) and angles (deg): Os(1)–N(1) = 2.167(4), Os(2)–N(5) = 2.175(4), Os(2)–N(4) = 2.261(4), Os(1)–N(2) = 2.225(4), N(2)–C(6) = 1.408(5), N(2)–C(7) = 1.324(6), N(3)–C(7) = 1.355(6), N(3)–C(14) = 1.373(5), N(4)–C(14) = 1.312(6), N(4)–C(15) = 1.411(6), P(1)–Os(1)–P(2) = 163.12(4), P(3)–Os(2)–P(4) = 164.51(4), N(1)–Os(1)–H(01) = 170.5(17), N(2)–Os(1)–C(21) = 164.71(19), N(4)–Os(2)–H(02) = 156.1(17), N(5)–Os(2)–C(22) = 171.30(18).

170.5(17)° and the carbonyl group located *trans* to the imine (N(2)–Os(1)–C(21) = 164.71(19)°). The other one, around the Os(2) atom, contains the hydride ligand *trans* to the imine (N(4)–Os(2)–H(02) = 156.1(17)°) and the carbonyl group *trans* to the pyridine (N(5)–Os(2)–C(22) = 171.30(18)°). With regard to the Os–N distances, the differences between the metal fragment are small, according to a similar *trans* influence for the hydride ligand and the carbonyl group. Thus, the osmium–pyridine bond lengths, 2.167(4) (Os(1)–N(1)) and 2.175(4) (Os(2)–N(5)) Å, are statistically identical, whereas the osmium–imine distance Os(2)–N(4) (2.261(4) Å, *trans* to hydride) is only 0.04 Å longer than the osmium–imine bond length Os(1)–N(2) (2.225(4) Å, *trans* to carbonyl). In accordance with the presence of two inequivalent metal fragments in the dimer, the ^1H NMR spectrum, in dichloromethane- d_2 , at room temperature shows two hydride resonances at –14.31 and –17.43 ppm, which are observed as triplets with H–P coupling constants of 20.0 and 18.8 Hz, respectively, whereas the $^{31}\text{P}\{^1\text{H}\}$ NMR spectrum exhibits two singlets at 20.6 and 20.2 ppm.

The $\mu\text{-(}\kappa^2\text{-N}_{\text{py}},\text{N}_{\text{imine}}\text{)}_2$ coordination mode is preferred not only for structures based on $\text{OsHX}(\text{P}^i\text{Pr}_3)_2$ (X = H₂, CO) skeletons but also for those supported for half-sandwich metal fragments such as $\text{OsCl}(\eta^6\text{-C}_6\text{H}_6)$. Treatment of dimer $\{\text{OsCl}(\eta^6\text{-C}_6\text{H}_6)\}_2(\mu\text{-Cl})_2$ (**8**) with 1.2 equiv of HBMePI, in methanol, at room temperature, for 48 h produces the precipitation of the red chloride salt of the cation $\text{trans-}[\{\text{OsCl}(\eta^6\text{-C}_6\text{H}_6)\}_2\{\mu\text{-(}\kappa^2\text{-N}_{\text{py}},\text{N}_{\text{imine}}\text{)}_2\text{-BMePI}\}]^+$ (**9a**, 56% yield), which indeed contains the polydentate anion coordinated in this way (**Scheme 5**). In contrast to **8**, its *p*-cymene

Scheme 5. Formation of **9a**



counterpart $\{\text{OsCl}(\eta^6\text{-p-cymene})\}_2(\mu\text{-Cl})_2$ (**10**) reacts with 1,3-bis(4'-tertbutyl-2'-pyridylimino)isoindoline in the presence of lithium diisopropylamide to afford a mononuclear $[\text{Os}\{\kappa^3\text{-N}_{\text{py}},\text{N}_{\text{iso}},\text{N}_{\text{py-fac}}\text{-(BPI)}\}(\eta^6\text{-p-cymene})]^+$ cation via a neutral $\text{OsCl}\{\kappa^2\text{-N}_{\text{py}},\text{N}_{\text{iso}}\text{-(BPI)}\}(\eta^6\text{-p-cymene})$ intermediate.¹⁰

The $\mu\text{-(}\kappa^2\text{-N}_{\text{py}},\text{N}_{\text{imine}}\text{)}_2$ coordination of BMePI in **9a** was confirmed by X-ray diffraction analysis. **Figure 6** shows a view of the structure. The cation has a C_2 axis, which crosses the isoindoline passing through the N(3) atom and the middle point of the C(10)–C(11) bond of the six-membered ring. As in the previous complexes, the osmium atoms are situated in position *anti* with regard to the isoindoline N(3) atom, with the arenes lying in different planes. One of them is located above the BMePI ligand, while the other one is situated below the anion. Thus, the coordination polyhedron around each osmium atom can be rationalized as a distorted octahedron with the arene occupying three sites of a face, whereas the pyridyl-imine unit (N(1)–Os(1)–N(2) = 61.17(16)°, N(5)–Os(2)–N(4) = 61.74(16)°) and the chloride ligand lie in the opposite one. The osmium–pyridine bond lengths of 2.117(4) (Os(1)–N(1)) and 2.097(4) (Os(2)–N(5)) Å and the osmium–imine distances of 2.156(4) (Os(1)–N(2)) and 2.152(4) (Os(2)–

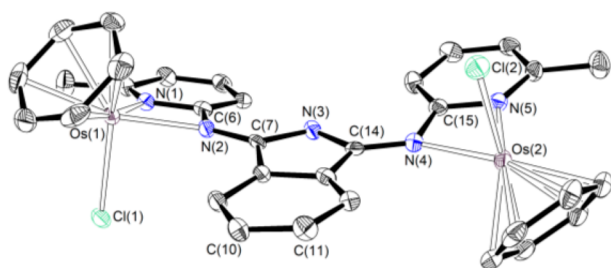
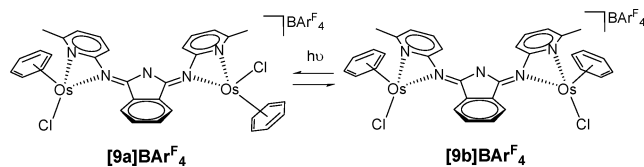


Figure 6. Molecular diagram of complex **9a** (50% probability ellipsoids). All hydrogen atoms are omitted for clarity. Selected bond lengths (Å) and angles (deg): Os(1)–N(1) = 2.117(4), Os(2)–N(5) = 2.097(4), Os(1)–N(2) = 2.156(4), Os(2)–N(4) = 2.152(4), N(2)–C(6) = 1.398(6), N(2)–C(7) = 1.314(6), N(3)–C(7) = 1.368(6), N(3)–C(14) = 1.354(6), N(4)–C(14) = 1.320(6), N(4)–C(15) = 1.411(6), N(1)–Os(1)–N(2) = 61.17(16), N(5)–Os(2)–N(4) = 61.74(16).

N(4)) Å compare well with the respective parameters in the previously mentioned compounds.

The $[\text{BAR}_4^{\text{F}}]^-$ salt of **9a** is very soluble in methanol, at room temperature, in contrast to the Cl^- salt. This methanol solution can be kept, at room temperature, under argon, in the absence of light, for a long time. However, under light, cation **9a** evolves to the *cis*-isomer **9b** (Scheme 6), to reach 1:1 equilibrium

Scheme 6. Light Mediated *trans-cis* (**9a-9b**) Isomerization for **9**



mixture, as a result of a 180° rotational process of one of the metal moieties around the closer imine N–C double bond. DFT calculations (B3LYP/def2-SVP level) have estimated an activation barrier of 16.2 kcal·mol^{−1} for the isomerization, the *trans* isomer being 0.6 kcal·mol^{−1} more stable than the *cis*-isomer.

The *cis* isomer **9b** has been also characterized by X-ray diffraction analysis. Figure 7 shows a view of its structure. The main difference with regard to **9a** is the presence of a symmetry

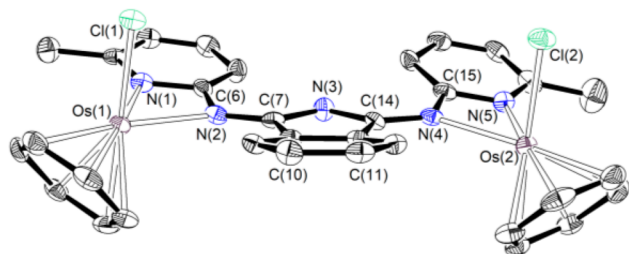
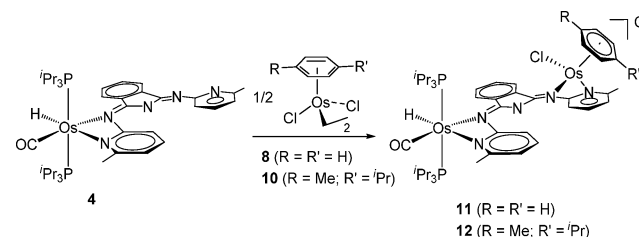


Figure 7. Molecular diagram of complex **9b** (50% probability ellipsoids). All hydrogen atoms are omitted for clarity. Selected bond lengths (Å) and angles (deg): Os(1)–N(1) = 2.096(5), Os(2)–N(5) = 2.110(5), Os(1)–N(2) = 2.142(5), Os(2)–N(4) = 2.149(5), N(2)–C(6) = 1.410(7), N(2)–C(7) = 1.313(7), N(3)–C(7) = 1.354(7), N(3)–C(14) = 1.361(7), N(4)–C(14) = 1.313(7), N(4)–C(15) = 1.407(7), N(1)–Os(1)–N(2) = 61.80(19), N(5)–Os(2)–N(4) = 61.58(18).

plane at the same position as the C_2 axis of **9a**. So, both arenes lie at the same face of the bridge ligand. The coordination polyhedron around the osmium is as in **9a**. The angles N(1)–Os(1)–N(2) and N(5)–Os(2)–N(4) of 61.80(19)° and 61.58(18)°, respectively, as well as the Os–pyridine bond lengths of 2.096(5) (Os(1)–N(1)) and 2.110(5) (Os(2)–N(5)) Å and the Os–imine distances of 2.142(5) (Os(1)–N(2)) and 2.149(5) (Os(2)–N(4)) Å agree well with the respective parameters of **9a**.

The fact that both metal fragments $\text{OsHX}(\text{P}^i\text{Pr}_3)_2$ and $\text{OsCl}(\eta^6\text{-C}_6\text{H}_6)$ prefer the $\kappa^2\text{-N}_{\text{py}}\text{N}_{\text{imine}}$ coordination prompted us to explore the possibility of forming heteroleptic species with the two different types of fragments connected by a $\mu\text{-(}\kappa^2\text{-N}_{\text{py}}\text{N}_{\text{imine}})_2\text{-BMePI}$ ligand. The free pyridine N(5) and imine N(4) atoms of **4** cleave the bridges of **8** and **10** and displace a chloride ligand of the resulting mononuclear fragment, to afford the desired heteroleptic dimer cations $[(\text{P}^i\text{Pr}_3)_2(\text{CO})\text{Hos}\{\mu\text{-(}\kappa^2\text{-N}_{\text{py}}\text{N}_{\text{imine}})_2\text{-BMePI}\}\text{OsCl}(\eta^6\text{-arene})]^+$ (arene = C_6H_6 (**11**), *p*-cymene (**12**)), which were isolated as both the red Cl^- and $[\text{BAR}_4^{\text{F}}]^-$ salts in high yield (87–92%), according to Scheme 7.

Scheme 7. Formation of **11** and **12**



The formation of these novel cations was confirmed by means of the X-ray analysis of the $[\text{BAR}_4^{\text{F}}]^-$ salt of **11**. The structure has two cations and two anions chemically equivalent but crystallographically independent in the asymmetric unit. Figure 8 shows a view of one of the cations. The coordination polyhedron around the Os(1) atom resembles that of **4** with P(1)–Os(1)–P(2), N(1)–Os(1)–H(01), and N(2)–Os(1)–C(39) angles of 162.03(8)° and 163.37(9)°, 160(3)° and 161(3)°, and 164.4(3)° and 165.8(3)°, respectively, whereas the geometry around Os(2) is also close to octahedral, with the arene occupying three sites of a face. The N(5), N(4)-pyridyl-imine unit, which acts with N(4)–Os(2)–N(5) bite angles of 61.9(3)° and 61.6(3)°, lies in the opposite sites along a chloride ligand. The Os(1)–pyridine bond lengths of 2.174(7) and 2.176(7) (Os(1)–N(1)) Å as well as the Os(1)–imine distances of 2.216(6) and 2.196(6) (Os(1)–N(2)) Å agree well with those of **4**, whereas the Os(2)–pyridine bond lengths of 2.118(7) and 2.100(8) (Os(2)–N(5)) Å and Os(2)–imine distances of 2.131(6) and 2.120(7) (Os(2)–N(4)) Å are between 0.05 and 0.08 Å shorter than the respective ones above-mentioned.

The ^1H and $^{31}\text{P}\{^1\text{H}\}$ NMR spectra of **11** and **12**, in dichloromethane- d_2 , at room temperature are consistent with the structure shown in Figure 8. In the ^1H NMR spectra, the most noticeable feature is a triplet ($^2J_{\text{H-P}} \approx 20$ Hz) at −14.39 ppm for **11** and at −14.50 ppm for **12**, corresponding to the hydride ligand. The $^{31}\text{P}\{^1\text{H}\}$ NMR spectra contains an AB spin system centered at 20.5 ppm and defined by $\Delta\nu = 169.5$ Hz and $^2J_{\text{P-P}} = 229.4$ Hz for **11** and by $\Delta\nu = 69.0$ Hz and $^2J_{\text{P-P}} = 229.1$ Hz for **12**, which indicates high activation barriers for

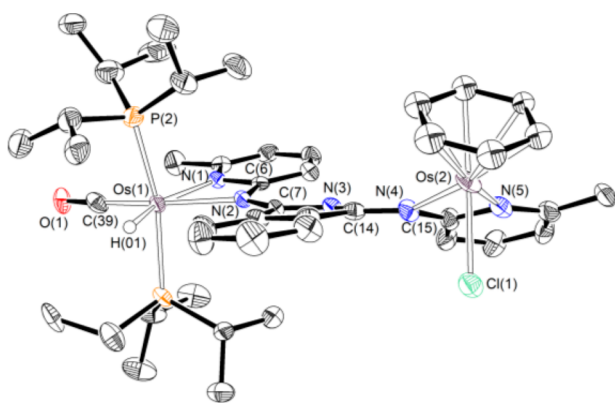


Figure 8. Molecular diagram of complex **11** (50% probability ellipsoids). All hydrogen atoms (except the hydride) are omitted for clarity. Selected bond lengths (Å) and angles (deg): Os(1)–N(1) = 2.174(7) and 2.176(7), Os(1)–N(2) = 2.216(6) and 2.196(6), Os(2)–N(5) = 2.118(7) and 2.100(8), Os(2)–N(4) = 2.131(6) and 2.120(7), N(2)–C(6) = 1.408(10) and 1.416(10), N(2)–C(7) = 1.324(10) and 1.322(10), N(3)–C(7) = 1.367(10) and 1.356(10), N(3)–C(14) = 1.333(10) and 1.347(10), N(4)–C(14) = 1.320(11) and 1.334(10), N(4)–C(15) = 1.383(11) and 1.380(11), P(1)–Os(1)–P(2) = 162.03(8) and 163.37(9), N(1)–Os(1)–H(01) = 160(3) and 161(3), N(2)–Os(1)–C(39) = 164.4(3) and 165.8(3), N(4)–Os(2)–N(5) = 61.9(3) and 61.6(3).

rotational processes around the imine N(2)–C(7) and N(4)–C(14) bonds.

The electronic properties of the heteroleptic complexes **11** and **12** were studied using experimental-computational methods. The homoleptic complex **9a** was also included in the study for comparison purposes. The electrochemical properties of these new class of bimetallic compounds were also addressed.

UV/vis absorption spectra of 1×10^{-5} M acetonitrile solutions of compounds **9a**, **11**, and **12** (Table 1, Table S1 and

Table 1. UV–Vis Excitation Energies (λ_{max} in nm) for Complexes **9a**, **11**, and **12**

complex	λ nm ($\epsilon \cdot 10^{-4}/\text{M}^{-1} \cdot \text{cm}^{-1}$) ^a
9a	498(2.08), 348(1.35), 279(3.02), 269(3.41)
11	480(3.74), 339 (2.53), 248 (5.36)
12	497(2.54), 338(1.89), 247(4.28)

^aData recorded at room temperature in acetonitrile with a concentration of 1×10^{-5} M. In parentheses, the molar extinction coefficient is ϵ .

Figure S1 in the Supporting Information) show an intense absorption band in the range 480–498 nm. Time-dependent DFT calculations (TD-B3LYP/def2-SVP, computed in acetonitrile as solvent) indicate that these visible transitions can be assigned to MLCT bands resulting from HOMO to LUMO or combinations of HOMO and HOMO–1 to LUMO transitions. The HOMOs are π -molecular orbitals mainly located at OsH(CO)(PⁱPr₃)₂ for **11** and **12** and at OsCl(η^6 -C₆H₆) for **9a**, whereas the LUMOs are π^* -molecular orbitals delocalized on BMePI ligand (Figure S2 in the Supporting Information). The UV–vis spectra also contain higher energy bands (λ = 330–340 nm), corresponding to combinations of electron transitions from orbitals below the HOMO to the LUMO.

Cyclic voltammetries (CV) for compounds **9a**, **11**, and **12** were conducted on 1×10^{-3} M acetonitrile solutions and 0.1 M

of the supporting electrolyte (Bu₄N)(ClO₄), and data are shown in Table 2. These compounds experience two reduction

Table 2. Electrochemical Data for Complexes **9a**, **11**, and **12**^a

	reduction		oxidation			
	E_{pc}^1	E_{pc}^2	E_{pa}^1	E_{pa}^2	E_{pa}^3	E_{pa}^4
9a	−0.75 ^b	−1.16	1.41	1.57		
11	−0.84 ^b	−1.32	0.92 ^b	1.15	1.35	1.48
12	−0.85 ^b	−1.35	0.92 ^b	1.23	1.43	1.82

^aData obtained from 1×10^{-3} M acetonitrile solutions, containing 0.1 M (Bu₄N)(ClO₄) as the supporting electrolyte at 20 °C. Data are given in V. Potentials are relative to Ag/AgCl. ^b $E_{1/2}$ values.

events. The first reduction wave is reversible (values ranging from −0.75 V to −0.84 V), and the second one is quasireversible, at values ranging from −1.16 V to −1.32 V. As the complexes studied have LUMO orbitals mainly centered on the BMePI moiety, the reduction appears to exclusively involve the bridging ligand (Figures S2 and S3 in the Supporting Information).

Heteroleptic complexes **11** and **12** display four oxidation events (Table 2). To get more information about the insights of these processes, a DFT investigation was conducted (B3LYP/def2-SVP level) using the model cation [(PMe₃)(CO)HOs{ μ -(κ^2 -N_{py},N_{imine})-BMePI}OsCl(η^6 -C₆H₆)}]⁺ (**11M**⁺; Figure 9). The results indicate that after the first reversible oxidation (at 0.92 V), the spin density for the one-electron oxidized species **11M**²⁺ is still predominantly resident on the OsH(CO)-(PMe₃)₂ metal fragment (0.75 e[−]). Subsequent loss of one electron (at 1.15 V) affords trication **11M**³⁺ showing a HOMO distribution with significant participation of the OsCl(η^6 -C₆H₆) metal fragment, from which the next oxidations at 1.35 and 1.48 V should take place. In consequence, the experimental and computational results indicate that the two metal fragments behave independently from each other in a sequential manner. The homoleptic cation **9a** shows two irreversible oxidation waves at 1.41 and 1.57 V, which agree well with the oxidations assigned to the OsCl(η^6 -C₆H₆) metal fragment of **11**.

Dehydrogenation of Alcohols and Amines Promoted by 3 and 4. Both complexes are efficient catalyst precursors for the acceptorless and base-free dehydrogenation of the above-mentioned hydrogen donors, including cyclic and lineal substrates. In contrast to **3** and **4**, diamine-phosphine osmium complexes previously reported require the use of KO^tBu for the reaction to proceed.¹⁵ The alcohol dehydrogenation was performed in toluene, at 100 °C, using a substrate concentration of 0.25 M and a 7% mol of catalyst, whereas the amine dehydrogenation was carried out in *p*-xylene, at 140 °C, using a substrate concentration of 0.12 M and a 10% mol of catalyst. Table 3 collects the alcohols studied and the yield of carbonyl compound formed after 24 h. Table 4 summarizes the results obtained, after 48 h, for the reactions performed with cyclic and lineal amines.

The trihydride complex **3** dehydrogenates 1-phenylethanol (run 1) and related alcohols with a substituent at the phenyl group (runs 3–5 and 7) to afford the corresponding ketones and H₂ (eq 1) in 60–80% yield, depending of the nature of the substituent and its position. A chloride substituent at the *para* position has a negligible influence (run 7), while a methyl group slightly favors the dehydrogenation. The influence of the position of the latter is however very marked, decreasing the

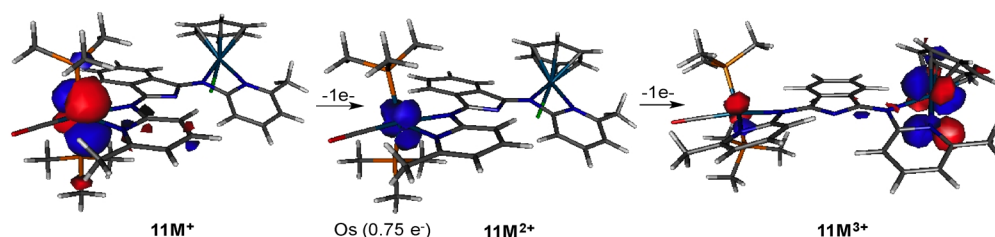


Figure 9. Computed (B3LYP/def2-SVP level) sequential two-electron oxidation of model heteroleptic complex $11M^+$: Highest occupied HOMO orbitals of $11M^+$ and $11M^{3+}$ and the spin density of dication $11M^{2+}$ (isosurface value 0.04).

amount formed of ketone as it approaches to the functional group; i.e., $p > m > o$ (runs $3 > 4 > 5$). For these substrates, the efficiency of the carbonyl complex **4** is comparable to that of the trihydride complex **3** (run 2 versus run 1 and run 6 versus run 5).

Complex **3** dehydrogenates diphenylmethanol (run 8) with the same efficiency as 1-*p*-tolylethanol; i.e., better than 1-phenylethanol. The adverse impact resulting from the increase of the steric hindrance due to the replacement of a methyl group in 1-phenylethanol by a phenyl appears to be compensated for the higher stability of benzophenone with regard to acetophenone. Diphenylmethanol is also better dehydrogenated than 1-phenylethanol in the presence of **4** (run 9), although the latter is slightly less active than **3**, in this case. The replacement of aryl substituents in the alcohol by alkyl groups certainly hampers the dehydrogenation. Thus, secondary alcohols with two alkyl groups, such as 2-octanol and 1-cyclohexylethanol (runs 10–13), are dehydrogenated worse (34–45%) than those containing some aromatic substituents. The same trend has been observed with other catalysts.^{3k} For these aliphatic substrates, the carbonyl complex **4** performs better than the trihydride derivative **3**. The latter also dehydrogenates functionalized alcohols such as 3-pyridylethanol (run 14), 4-pyridylethanol (run 15), and 1-(tetrahydrofuran-2-yl)ethan-1-ol (run 16). The corresponding ketones are formed in 20–45% yield. The position of the CH_3CHOH -group at the pyridyl ring has a noticeable influence in the reaction; the conversion to the ketone increases as the substituent approaches the nitrogen atom. In agreement with this, Nakazawa and co-workers have observed that while a wide range of 2-pyridylmethanol derivatives is efficiently dehydrogenated with the iron precursor $Fe(\eta^5-C_5H_5)Cl(CO)_2$ and NaH, 3-pyridylmethanol and 4-pyridylmethanol do not undergo oxidation under the same conditions.^{7c}

Complex **3** transforms primary alcohols, such as benzyl alcohol (run 17), 4-methylbenzyl alcohol (run 19), and 4-chlorobenzyl alcohol (run 20), into the corresponding aldehyde and H_2 . The amount of ester formed, as a consequence of a dehydrogenative alcohol dimerization is lower than 8% in all cases. In contrast to **3**, osmium complexes stabilized by P,N,P -, P,N,N -, and N,N,N -pincer ligands afford esters.^{14b,e} A similar behavior has been also observed for $RuH_2(PPh_3)_4$ related ruthenium precursors stabilized by pincer^{3f} and tetradentate amine-phosphines and pincer N,N,N ligands,^{3h} and P,N,P -iron derivatives.^{7b} Both electron withdrawing and electron donating groups favor the dehydrogenation. Thus, substituted benzaldehydes are formed in better yields than benzaldehyde. The carbonyl complex **4** is also active for the dehydrogenation of benzyl alcohol (run 18), although it is less efficient than the trihydride complex **3**.

Heterocycles containing nitrogen include 1,2,3,4-tetrahydroquinoline, 1,2,3,4-tetrahydroquinoline, 6-methyl-1,2,3,4-tetrahydroquinoline, 1,2,3,4-tetrahydroisoquinoline, and 2-methylindoline. Both complexes **3** and **4** are efficient catalyst precursors to promote the dehydrogenation of these substrates. Under the reaction conditions the aromatic heterocycles were formed with yields between 100% and 18%. The amount of molecular hydrogen released per gram of heterocycle used, after 48 h, depends upon three factors: (i) the presence of a methyl group adjacent to the nitrogen atom, (ii) the position of the heteroatom in the heterocycle, and (iii) the size of the heterocycle.

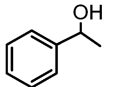
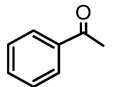
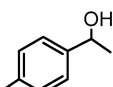
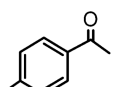
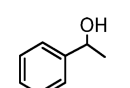
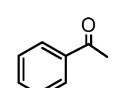
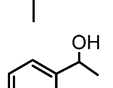
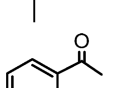
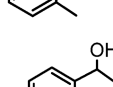
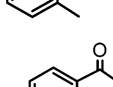
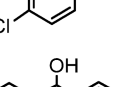
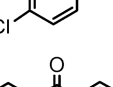
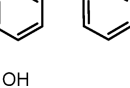
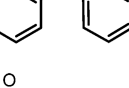
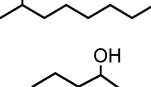
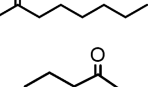
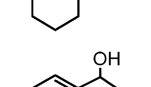
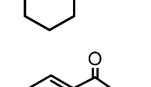
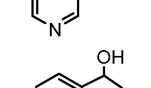
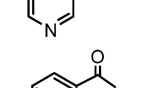
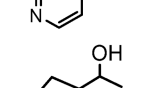
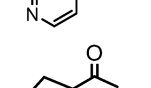
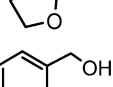
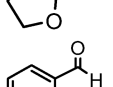
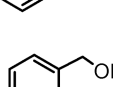
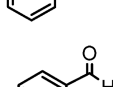
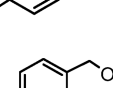
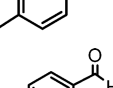
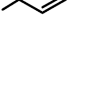
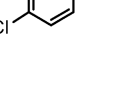
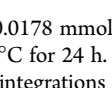
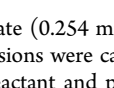
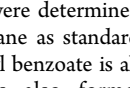
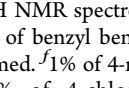
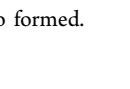



A methyl group adjacent to the nitrogen atom hampers the dehydrogenation. While 1,2,3,4-tetrahydroquinoline (runs 1 and 2) and 6-methyl-1,2,3,4-tetrahydroquinoline (runs 5 and 6) afford the corresponding quinolines in 68–85% yield, releasing between 1.02×10^{-2} and 1.22×10^{-2} mol·g⁻¹ of H_2 , quinaldine (runs 3 and 4) is formed in 18–31% yield along 0.24 – 0.42×10^{-2} mol·g⁻¹ of H_2 . Since the presence of the methyl substituent adjacent to the heteroatom reduces the coordination ability of the heterocycle, this reveals that the coordination of the nitrogen atom to the metal center of the catalysts is a key step in the dehydrogenation. The position of the heteroatom in the heterocycle certainly plays an important role for the catalysis. Thus, 1,2,3,4-tetrahydroisoquinoline (runs 7 and 8) is dehydrogenated worse than 1,2,3,4-tetrahydroquinoline. After 48 h in the presence of **3**, the former releases 0.78×10^{-2} mol·g⁻¹ of H_2 , about 34% less than 1,2,3,4-tetrahydroquinoline. This is in contrast with that previously observed for the acetylacetonate derivative $OsH_3(acac)(P^iPr_3)_2$.¹⁶ Under the same conditions, with this catalyst, 1,2,3,4-tetrahydroisoquinoline releases 1.50×10^{-2} mol·g⁻¹ of H_2 , about 20% more than 1,2,3,4-tetrahydroquinoline (1.20×10^{-2} mol·g⁻¹). A similar behavior has been observed for some ruthenium-hydride precursors.^{3g} The size of the heterocycle is also relevant. 2-Methylisindoline (runs 9 and 10) releases all its capacity of H_2 , 0.84×10^{-2} mol·g⁻¹, between 70% and 50% more than the molecular hydrogen produced from its six-membered counterpart 1,2,3,4-tetrahydroquinoline.

Complexes **3** and **4** also promote the dehydrogenation of lineal amines such as *N*-phenylbenzylamine (runs 11 and 12) and *N*-methylbenzylamine (run 13) to afford the corresponding imines in 37%–16% yield, after 48 h reaction.

CONCLUDING REMARKS

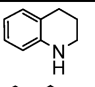
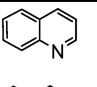
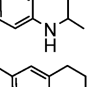
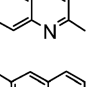
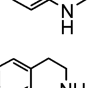
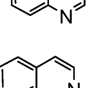
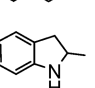
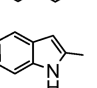
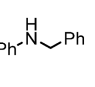
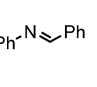
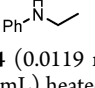
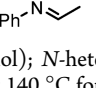
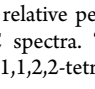
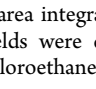
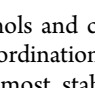
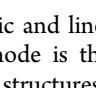
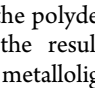
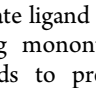
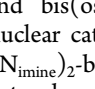
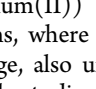
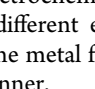
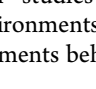
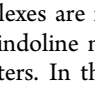
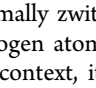
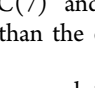
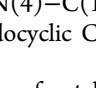
This study has revealed that the anion 1,3-bis(6-methyl-2-pyridylimino)-isoindolate, with five-basic nitrogen atoms, coordinates to osmium(IV) and osmium(II) metal fragments in the unprecedented $\kappa^2-N_{py}N_{imine}$ fashion to form mononuclear complexes, which are efficient catalyst precursors for the acceptorless and base-free dehydrogenation of secondary

Table 3. Osmium Catalyzed Acceptorless and Base-Free Dehydrogenation of Alcohols^a

run	catalyst	substrate	product	yield (%) ^b
1	3			60
2	4			60
3	3			76
4	3			63
5	3			39
6	4			39
7	3			61
8	3			77
9	4			69
10	3			34
11	4			46
12	3			37
13	4			45
14	3			32
15	3			20
16	3			45
17 ^c	3			31 ^{c,d}
18 ^c	4			13 ^{c,e}
19 ^c	3			58 ^{c,f}
20 ^c	3			41 ^{c,g}

^aConditions: **3** or **4** (0.0178 mmol); substrate (0.254 mmol); toluene (1 mL) heated at 100 °C for 24 h. ^bConversions were calculated from the relative peak area integrations of the reactant and product in the GC spectra. ^cYields were determined by ¹H NMR spectroscopy using 1,1,2,2-tetrachloroethane as standard. ^d3% of benzyl benzoate is also formed. ^e7% of benzyl benzoate is also formed. ^f1% of 4-methylbenzyl 4-methylbenzoate is also formed. ^g8% of 4-chlorobenzyl 4-chlorobenzoate is also formed.

Table 4. Osmium Catalyzed Acceptorless and Base-Free Dehydrogenation of N-Heterocycles and Lineal Amines^a

run	catalyst	substrate	product	yield (%) ^b	mol H ₂ /g substrate
1	3			81	1.22 · 10 ⁻²
2	4			68	1.02 · 10 ⁻²
3	3			18	0.59 · 10 ⁻²
4	4			31	0.42 · 10 ⁻²
5	3			85	1.15 · 10 ⁻²
6	4			78	1.06 · 10 ⁻²
7	3			52	0.78 · 10 ⁻²
8	4			51	0.77 · 10 ⁻²
9	3			100	0.84 · 10 ⁻²
10	4			100	0.84 · 10 ⁻²
11 ^c	3			37	0.20 · 10 ⁻²
12 ^c	4			26	0.14 · 10 ⁻²
13 ^c	3			16	0.13 · 10 ⁻²

^aConditions: **3** or **4** (0.0119 mmol); N-heterocyclic substrate (0.119 mmol); *p*-xylene (1 mL) heated at 140 °C for 48 h. ^bConversions were calculated from the relative peak area integrations of the reactant and product in the GC spectra. ^cYields were determined by ¹H NMR spectroscopy using 1,1,2,2-tetrachloroethane as standard.

and primary alcohols and cyclic and lineal amines. The reason for this novel coordination mode is thermodynamic, since it gives rise to the most stable structures from all the possible options. Because the polydentate ligand still has three free basic nitrogen atoms, the resulting mononuclear species can be further used as metalloligands to prepare homoleptic bis-(osmium(IV)) and bis(osmium(II)) and heteroleptic bis-(osmium(II)) dinuclear cations, where the polydentate ligand acts as μ -(κ^2 -N_{py}-N_{imine})₂-bridge, also unprecedented. Frontier orbitals and electrochemical studies on bis(osmium(II)) complexes, with different environments around each osmium atom, show that the metal fragments behave independently and in a sequence manner.

The new complexes are formally zwitterions with a negative charge on the isoindoline nitrogen atom and a positive charge on the metal centers. In this context, it should be noted that exocyclic N(2)–C(7) and N(4)–C(14) bond lengths are generally shorter than the endocyclic C(7)–N(3) and N(3)–C(14) distances.

In conclusion, a novel type of catalyst precursors for the acceptorless and base-free dehydrogenation of hydrogen carriers based on organic liquids, which can be further employed as metalloligands to generate homoleptic and heteroleptic dinuclear metal cations, has been discovered.

EXPERIMENTAL SECTION

All reactions were carried out with rigorous exclusion of air using Schlenk-tube techniques. Acetone, methanol, tetrahydrofuran, 2-propanol, and *p*-xylene were dried and distilled under argon. Other solvents were obtained oxygen- and water-free from an MBraun solvent purification apparatus. NMR spectra were recorded on a Varian Gemini 2000, a Bruker ARX 300 MHz, a Bruker Avance 300 MHz, or a Bruker Avance 400 MHz instrument. Chemical shifts (expressed in parts per million) are referenced to residual solvent peaks (¹H, ¹H{³¹P}, ¹³C{¹H}) or external standard (³¹P{¹H}) to 85%

H₃PO₄ and ¹¹B to BF₃·OEt₂). Coupling constants *J* and *N* (*N* = *J*(PH) + *J*(P'H) for ¹H and *N* = *J*(PC) + *J*(P'C) for ¹³C{¹H}) are given in hertz. Attenuated total reflection infrared spectra (ATR-IR) of solid samples were run on a PerkinElmer Spectrum 100 FT-IR spectrometer. C, H, and N analyses were carried out in a PerkinElmer 2400 CHNS/O analyzer. High-resolution electrospray mass spectra (HRMS) were acquired using a MicroTOF-Q hybrid quadrupole time-of-flight spectrometer (Bruker Daltonics, Bremen, Germany). Cyclic voltammograms (CVs) were recorded at room temperature in acetonitrile solutions using concentrations 1.10^{−3} M of the test sample and 0.1 M of the supporting electrolyte (Bu₄N)(ClO₄), in an Autolab PGSTAT302N potentiostat with Ag/AgCl 3 M as reference electrode and Pt and glassy carbon as the counter and working electrodes, respectively (scan rate 0.1 V/s). All reagents and substrates were purchased from commercial sources and were dried and distilled under argon or in a Kugelrohr distillation oven. 5-*tert*-Butyl-4-hydroxy-2-methylphenyl sulfide was purchased from commercial sources and used without further purification. OsH₆(P'Pr₃)₂ (**1**),³¹ OsHCl(CO)-(P'Pr₃)₂,³² OsH(OH)(CO)(P'Pr₃)₂ (**2**),³³ OsH₂Cl₂(P'Pr₃)₂ (**5**),³¹ [(η⁶-C₆H₆)OsCl₂]₂ (**8**),³⁴ [(η⁶-*p*-cymene)OsCl₂]₂ (**10**),³⁵ and 1,3-bis(6-methylpyridyl-2-imino)isoindoline (HBPI)³⁶ were prepared according to the published methods. The formed imines were characterized by comparison of their ¹H NMR spectra with those previously reported: *N*-benzylidene aniline^{14a} and *N*-(phenylmethylene)methanamine.³⁷ The formed aldehydes were characterized by comparison of their ¹H NMR spectra with those previously reported: 4-methylbenzaldehyde³⁸ and 4-chlorobenzaldehyde.³⁸

OsH₃(κ²-N_{py}N_{imine}-(BMePI))(P'Pr₃)₂ (3**).** OsH₆(P'Pr₃)₂ (0.100 g, 0.193 mmol) was dissolved in propan-2-ol (10 mL) and treated with 1,3-bis(6'-methyl-2'-pyridylimino)isoindoline (HBMePI) (0.063 g, 0.193 mmol). The yellow solution was stirred under reflux for 6 h, and then the volatiles were removed under vacuum. The resulting residue was precipitated and washed with pentane (3 × 3 mL, 233 K) affording a red solid which was dried *in vacuo*. Yield: 0.108 mg (67%). Red crystals suitable for X-ray diffraction analysis were obtained from slow diffusion of pentane in a concentrated solution of **3** in toluene. Anal. Calcd. for C₃₈H₆₁N₅O₂OsP₄: C, 54.33; H, 7.32; N, 8.34. Found: C, 54.62; H, 7.07; N, 8.48. HRMS (electrospray, *m/z*): Calcd. for C₃₈H₆₁N₅O₂OsP₄ [M + H]⁺: 842.4092, found: 842.4150. ¹H NMR (300 MHz, CD₂Cl₂, 298 K): δ 9.05 (d, ³J_{H-H} = 6.3, 1 H, CH_{arom}), 8.56 (d, ³J_{H-H} = 8.4, 1 H, CH_{arom}), 7.92 (dd, ³J_{H-H} = 6.0, ³J_{H-H} = 1.5, 1 H, CH_{arom}), 7.55 (d, ³J_{H-H} = 8.0, 1 H, CH_{arom}), 7.35 (t, ³J_{H-H} = 7.6, 1 H, CH_{arom}), 7.30 (dt, ³J_{H-H} = 7.5, ¹J_{H-H} = 1.0, 1 H, CH_{arom}), 7.16 (dt, ³J_{H-H} = 7.4, ¹J_{H-H} = 0.8, 1 H, CH_{arom}), 7.11 (t, ³J_{H-H} = 8.1, 1 H, CH_{arom}), 6.63 (d, ³J_{H-H} = 7.3, 1 H, CH_{arom}), 6.26 (d, ³J_{H-H} = 7.4, 1 H, CH_{arom}), 2.54 (s, 3 H, py-CH₃), 2.23 (s, 3 H, py-CH₃), 1.89 (m, 6 H, PCH), 0.87 (dvt, ³J_{H-H} = 6.8, *N* = 12.8, 36 H, PCH(CH₃)₂), −12.06 (br, 3 H, OsH). ¹H NMR (300 MHz, CD₂Cl₂, 193 K): δ −10.68 (d, ³J_{H-H} = 66.6, 1 H), −12.15 (dd, ³J_{H-H} = 66.6, ³J_{H-H} = 37.1), −13.89 (d, ³J_{H-H} = 37.1). T₁(min) (ms, OsH, 300 MHz, CD₂Cl₂, 203 K): 91 (−10.68 ppm). ¹³C{¹H} NMR (75.5 MHz, CD₂Cl₂, 298 K): δ 171.9, 166.8, 166.7, 164.1, 157.8, 155.1, 142.4, 140.4 (all s, C_{arom}), 137.6, 137.2, 130.1, 129.1, 123.0, 122.1, 118.8, 117.6, 116.7, 116.4 (all s, CH_{arom}), 28.7 (dvt, PCH), 25.3 and 25.1 (both s, CH₃), 20.5 and 20.3 (both s, PCH(CH₃)₃). ³¹P{¹H} NMR (121 MHz, CD₂Cl₂, 298 K): δ 20.1 (s).

OsH(κ²-N_{py}N_{imine}-(BMePI))(CO)(P'Pr₃)₂ (4**).** OsH(OH)(CO)-(P'Pr₃)₂ (**2**) (0.070 g, 0.126 mmol) was dissolved in toluene (5 mL) and treated with HBPI (0.045 g, 0.138 mmol). The mixture was stirred for 2 h at room temperature before the volatiles were removed under vacuum. The residue was washed with methanol (2 × 1 mL) at approximately 203 K and dried under vacuum affording an orange solid. Yield: 0.065 g (60%). A crystal suitable for X-ray diffraction study was obtained from slow diffusion of methanol in a concentrated solution of **2** in toluene. Anal. Calcd. for C₃₉H₅₉N₅O₃OsP₂·CH₃OH: C, 53.49; H, 7.07; N, 7.80. Found: C, 53.15; H, 6.86; N, 7.73. HRMS (electrospray, *m/z*): Calcd. for C₃₉H₆₀N₅O₃OsP₂ [M + H]⁺: 868.3885, found: 868.3903. IR (cm^{−1}): ν (CO) 1885 (s). ¹H NMR (300 MHz, CD₂Cl₂, 298 K): δ 8.83 (d, ³J_{H-H} = 7.3, 1H, CH_{arom}), 8.43 (d, ³J_{H-H} =

8.4, 1H, CH_{arom}), 7.89 (d, ³J_{H-H} = 7.2, 1H, CH_{arom}), 7.54 (dd, ³J_{H-H} = 8.0, 7.5, 1H, CH_{arom}), 7.46 (dd, ³J_{H-H} = 8.4, 6.9 1H, CH_{arom}), 7.45 (dd, ³J_{H-H} = 7.2, 6.9 1H, CH_{arom}), 7.37 (dd, ³J_{H-H} = 7.5, 7.3, 1H, CH_{arom}), 7.31 (d, ³J_{H-H} = 8.0, 1H, CH_{arom}), 6.84 (d, ³J_{H-H} = 6.9, 1H, CH_{arom}), 6.82 (d, ³J_{H-H} = 6.9, 1H, CH_{arom}), 2.60 (s, 3H, py-CH₃), 2.51 (s, 3H, py-CH₃), 2.43–2.27 (m, 6H, PCH), 1.12 (dvt, *N* = 12.9, ³J_{H-H} = 6.9, 18H, PCH(CH₃)₂), 1.04 (dvt, *N* = 13.2, ³J_{H-H} = 6.9, 18H, PCH(CH₃)₂), −14.00 (t, ²J_{H-P} = 20.3 Os–H, 1H). ¹³C{¹H} NMR (75.5 MHz, CD₂Cl₂, 298 K): δ 186.6 (t, ²J_{C-P} = 9.7, CO), 171.9, 168.4, 167.8, 163.5, 157.7, 156.7, 141.5, 139.2 (all s, C_{arom}), 137.2, 137.1, 130.4, 128.8, 123.6, 121.9, 118.9, 117.8, 116.2, 116.1 (all s, CH_{arom}), 28.0 (vt, *N* = 24.8, PCH), 25.1 (s, py-CH₃), 24.8 (s, py-CH₃), 20.1 (s, PCH(CH₃)₂). ³¹P{¹H} NMR (121 MHz, CD₂Cl₂, 298 K): δ 19.5 (s).

Synthesis of [(OsH₃(P'Pr₃)₂)₂(μ-(κ²-N_{py}N_{imine})₂-BMePI)]Cl (**6**).

A yellow solution of HBMePI (31 mg, 0.094 mmol) in propan-2-ol (10 mL) was treated with ^tBuOK (12 mg, 0.103 mmol) and stirred for 30 min at room temperature. Then, OsH₂Cl₂(P'Pr₃)₂ (0.100 g, 0.170 mmol) was added, and the resulting suspension was stirred for 4 h at room temperature. The volatiles were removed under vacuum, and the residue was recrystallized with toluene and filtered through a column of Celite. The solvent was removed under vacuum, and the resulting residue was precipitated and washed with pentane (3 × 3 mL, 233 K) affording a dark-purple solid. Yield: 49%. Crystals of **6** suitable for X-ray diffraction study were obtained from C₆D₆, using 5-*tert*-butyl-4-hydroxy-2-methylphenyl sulfide to facilitate the crystallization by the formation of intermolecular hydrogen bonds. HRMS (electrospray, *m/z*): Calcd. for C₅₆H₁₀₆N₅O₂P₄ [M]⁺: 1354.6605, found: 1354.6553. ¹H NMR (300 MHz, CD₂Cl₂, 298 K): δ 9.19 (m, 2 H, CH_{arom}), 8.45 (d, ³J_{H-H} = 8.4, 2 H, CH_{arom}), 7.73 (t, ³J_{H-H} = 8.0, 2 H, CH_{arom}), 7.55 (m, 2 H, CH_{arom}), 7.11 (d, ³J_{H-H} = 7.6, 2 H, CH_{arom}), 2.58 (s, 6 H, py-CH₃), 2.07 (m, 6 H, PCH), 1.00 (dvt, ³J_{H-H} = 6.8, *N* = 12.6, 36 H, PCH(CH₃)₂), −12.18 (t, ²J_{H-P} = 12.2, 6 H, OsH). ¹H NMR (300 MHz, CD₂Cl₂, 193 K): δ −10.78 (d, *J* = 168, 2 H), −12.11 (d, *J* = 170, 2 H), −13.95 (br, 2 H). T₁(min) (ms, OsH, 300 MHz, CD₂Cl₂, 233 K): 70 (−12.65 ppm). ¹³C{¹H} NMR (75.5 MHz, CD₂Cl₂, 298 K): δ 167.2, 165.2, 156.5, 139.8 (all s, C_{arom}), 138.1, 130.5, 124.2, 122.0, 116.4 (all s, CH_{arom}), 28.7 (vt, *N* = 12.1, PCH), 25.4 (s, CH₃), 20.3 and 20.1 (both s, PCH(CH₃)₃). ³¹P{¹H} NMR (121 MHz, CD₂Cl₂, 298 K): δ 20.9 (s).

[(OsH(CO)(P'Pr₃)₂)₂(μ-(κ²-N_{py}N_{imine})₂-BMePI)]BF₄ (7**).** A solution of OsHCl(CO)(P'Pr₃)₂ (0.046 g, 0.080 mmol) in acetone (5 mL) was treated with AgBF₄ (0.016 g, 0.082 mmol) and stirred for 30 min at room temperature. Then, **4** was added (0.070 g, 0.080 mmol), and the solution was stirred for 3 h at room temperature. The suspension was filtered through Celite, the volatiles were removed under vacuum, and the residue was washed with diethyl ether (2 × 2 mL) affording a dark purple solid, which is a mixture of isomers **7a** and **7b** (ratio 0.4:1). Yield: 0.081 g (67%). Crystals of both isomers suitable for X-ray diffraction study were obtained from slow diffusion of diethyl ether in a concentrated solution of **7a** + **7b** in dichloromethane. Anal. Calcd. for BC₅₈F₄H₁₀₂N₅O₂Os₂P₄: C, 46.67; H, 6.89; N, 4.69. Found: C, 46.37; H, 6.56; N, 4.72. HRMS (electrospray, *m/z*): Calcd. for C₅₈H₁₀₂N₅O₂Os₂P₄ [M]⁺: 1406.6190, found: 1406.6155. IR (cm^{−1}): ν (CO) 1887 (s). Complex **7a**: ¹H NMR (400 MHz, CD₂Cl₂, 298 K) δ 8.98 (d, ³J_{H-H} = 4.0, 2H, CH_{arom}), 8.29 (d, ³J_{H-H} = 7.2, 2H, CH_{arom}), 7.74 (dd, ³J_{H-H} = 7.6, 7.2, 2H, CH_{arom}), 7.50 (dd, ³J_{H-H} = 4.4, 4.0, 2H, CH_{arom}), 7.13 (d, ³J_{H-H} = 7.6, 2H, CH_{arom}), 2.66 (s, 6H, py-CH₃), 2.37–2.27 (m, 6H, PCH), 1.18–1.09 (m, 36H, PCH(CH₃)₂), 1.05 (dvt, *N* = 13.2, ³J_{H-H} = 7.2, 36H, PCH(CH₃)₂), −14.45 (t, ²J_{H-P} = 20.0 Os–H, 2H). ¹³C{¹H} NMR (100.6 MHz, CD₂Cl₂, 298 K): δ 185.8 (t, ²J_{C-P} = 9.2, CO), 168.9, 166.3, 158.4, 139.5 (all s, C_{arom}), 138.0, 131.0, 125.0, 122.7, 116.2 (all s, CH_{arom}), 27.6 (vt, *N* = 24.9, PCH), 24.8 (s, py-CH₃), 20.1 and 19.4 (both s, PCH(CH₃)₂). ³¹P{¹H} NMR (162 MHz, CD₂Cl₂, 298 K): δ 20.2 (s). Complex **7b**: ¹H NMR (400 MHz, CD₂Cl₂, 298 K) δ 8.97 (d, ³J_{H-H} = 7.6, 1H, CH_{arom}), 8.51 (d, ³J_{H-H} = 7.6, 1H, CH_{arom}), 8.46 (d, ³J_{H-H} = 8.4, 1H, CH_{arom}), 8.30 (d, ³J_{H-H} = 7.6, 1H, CH_{arom}), 7.82 (dd, ³J_{H-H} = 8.4, 7.6, 1H, CH_{arom}), 7.72 (dd, ³J_{H-H} = 7.6, 7.6 1H, CH_{arom}), 7.58 (dd, ³J_{H-H} =

7.6, 7.2, 1H, CH_{arom}), 7.50 (dd, ³J_{H-H} = 7.6, 7.2, 1H, CH_{arom}), 7.13 (d, ³J_{H-H} = 7.6, 1H, CH_{arom}), 7.09 (d, ³J_{H-H} = 7.6, 1H, CH_{arom}), 2.66 (s, 3H, py-CH₃), 2.47 (s, 3H, py-CH₃), 2.37–2.27 (m, 6H, PCH), 2.27–2.18 (m, 6H, PCH), 1.18–1.09 (m, 36H, PCH(CH₃)₂), 1.05 (dvt, N = 12.8, ³J_{H-H} = 6.4, 18H, PCH(CH₃)₂), 0.98 (dvt, N = 12.8, ³J_{H-H} = 6.8, 18H, PCH(CH₃)₂), –14.31 (t, ²J_{H-P} = 20.0, Os-H, 1H), –17.43 (t, ²J_{H-P} = 18.8, Os-H, 1H). ¹³C{¹H} NMR (100.6 MHz, CD₂Cl₂, 298 K): δ 187.7 (t, ²J_{C-P} = 9.8, CO), 185.8 (t, ²J_{C-P} = 9.4, CO), 171.0, 168.9, 167.3, 166.6, 158.2, 156.8 (all s, C_{arom}), 140.0 (s, CH_{arom}), 139.5, 138.4 (both s, C_{arom}), 137.8, 131.3, 130.3, 125.1, 124.9, 122.1, 122.0, 117.5, 116.0 (all s, CH_{arom}), 28.1 (vt, N = 24.9, PCH), 28.0 (vt, N = 24.5, PCH), 25.2 (s, py-CH₃), 25.1 (s, py-CH₃), 20.2 and 20.1 (both s, PCH(CH₃)₂). ³¹P{¹H} NMR (162 MHz, CD₂Cl₂, 298 K): δ 20.6 and 20.2 (both s).

trans-[(OsCl(η⁶-C₆H₆))₂μ-(κ²-N_{py},N_{imine})₂-BMePI]Cl (9a)Cl. A solution of [(η⁶-C₆H₆)OsCl₂]₂ (8) (0.100 g, 0.147 mmol) in methanol (5 mL) was treated with HBPI (0.058 g, 0.177 mmol) and stirred for 48 h at room temperature in the absence of light. After this time, a red solid had precipitated, and the solution was removed. The volatiles were removed under vacuum, and the red solid was washed with diethyl ether (3 × 2 mL) and dried under vacuum. Yield: 0.085 g (59%). A crystal suitable for X-ray diffraction study was obtained from a concentrated solution of 9a in dichloromethane. It was not possible to measure ¹³C spectrum due to low solubility of the complex. Isomer *trans* was obtained. Anal. Calcd. for C₃₂Cl₃H₂₈N₅O₅: C, 39.65; H, 2.91; N, 7.22. Found: C, 39.82; H, 2.79; N, 7.03. ¹H NMR (300 MHz, CD₂Cl₂, 298 K): δ 8.36 (dd, ³J_{H-H} = 5.6, ⁴J_{H-H} = 3.1, 2H, CH_{arom}), 7.81 (dd, ³J_{H-H} = 8.4, 7.7, 2H, CH_{arom}), 7.72 (d, ³J_{H-H} = 8.4, 2H, CH_{arom}), 7.68 (dd, ³J_{H-H} = 5.6, ⁴J_{H-H} = 3.1, 2H, CH_{arom}), 7.13 (d, ³J_{H-H} = 7.7, 2H, CH_{arom}), 6.32 (s, 12H, η⁶-C₆H₆), 2.69 (s, 6H, py-CH₃).

[(OsCl(η⁶-C₆H₆))₂μ-(κ²-N_{py},N_{imine})₂-BMePI](BAR^F₄) (9a)BAR^F₄ + [9b]BAR^F₄. A suspension of [9a]Cl (0.085 g, 0.088 mmol) in methanol (5 mL) was treated with NaBAR^F₄ (0.093 g, 0.105 mmol) and stirred for 3 h, at room temperature under light. The volatiles of the resulting red solution were removed under vacuum, and 10 mL of dichloromethane was added. The solution was filtered through Celite and dried under vacuum. The residue was washed with pentane (3 × 2 mL) at approximately 203 K affording an orange solid, which was a mixture of [BAR^F₄][−] salts of the cations 9a and 9b in about a 1:1 ratio. Yield: 0.126 g (80%). A crystal of 9b suitable for X-ray diffraction study was obtained from slow diffusion of pentane in a concentrated solution of the mixture in dichloromethane. Anal. Calcd. for BC₆₄Cl₂F₂₄H₄₀N₅O₅: C, 42.77; H, 2.24; N, 3.90. Found: C, 42.88; H, 2.60; N, 3.51. HRMS (electrospray, *m/z*): Calcd. for C₃₂Cl₂H₂₈N₅O₅ [M]⁺: 934.0900, found: 934.0947. Isomer *trans* (9a): ¹H NMR (300 MHz, CD₂Cl₂, 298 K) δ 8.39 (dd, ³J_{H-H} = 5.6, ⁴J_{H-H} = 3.1, 2H, CH_{arom}), 7.81–7.67 (m, 14H, CH_{arom} (BPI + BAR^F₄)), 7.56 (s, 4H, CH_{arom} (BAR^F₄)), 7.06 (d, ³J_{H-H} = 8.0, 2H, CH_{arom}), 6.16 (s, 12H, η⁶-C₆H₆), 2.64 (s, 6H, py-CH₃). ¹³C{¹H} NMR (75.5 MHz, CD₂Cl₂, 298 K): δ 171.7, 166.3 (both s, C_{arom}), 162.3 (q, ¹J_{B-C} = 49.8, C(BAR^F₄)), 157.2 (s, C_{arom}), 141.3 (s, CH_{arom}), 139.0 (s, C_{arom}), 135.4 (s, CH_{arom} (BAR^F₄)), 133.0 (s, CH_{arom}), 129.4 (qq, ²J_{C-F} = 31.5, ³J_{C-B} = 2.8, C-CF₃ (BAR^F₄)), 125.2 (q, ¹J_{C-F} = 272.5, CF₃ (BAR^F₄)), 125.0, 122.1 (both s, CH_{arom}), 118.1 (spt, ³J_{C-F} = 3.9, CH_{arom} (BAR^F₄)), 116.1 (s, CH_{arom}), 76.1 (s, η⁶-C₆H₆), 23.3 (s, py-CH₃). Isomer *cis* (9b): ¹H NMR (300 MHz, CD₂Cl₂, 298 K) δ 8.34 (dd, ³J_{H-H} = 5.6, ⁴J_{H-H} = 3.1, 2H, CH_{arom}), 8.06 (d, ³J_{H-H} = 8.5, 2H, CH_{arom}), 7.81–7.67 (m, 12H, CH_{arom} (BPI + BAR^F₄)), 7.56 (s, 4H, CH_{arom} (BAR^F₄)), 7.12 (d, ³J_{H-H} = 8.9, 2H, CH_{arom}), 6.16 (s, 12H, η⁶-C₆H₆), 2.67 (s, 6H, py-CH₃). ¹³C{¹H} NMR (75.5 MHz, CD₂Cl₂, 298 K): δ 171.7, 166.7 (both s, C_{arom}), 162.3 (q, ¹J_{B-C} = 49.8, C(BAR^F₄)), 157.0 (s, C_{arom}), 141.2 (s, CH_{arom}), 138.7 (s, C_{arom}), 135.4 (s, CH_{arom} (BAR^F₄)), 132.6 (s, CH_{arom}), 129.4 (qq, ²J_{C-F} = 31.5, ³J_{C-B} = 2.8, C-CF₃ (BAR^F₄)), 125.2 (q, ¹J_{C-F} = 272.5, CF₃ (BAR^F₄)), 124.6, 122.0 (both s, CH_{arom}), 118.1 (spt, ³J_{C-F} = 3.9, CH_{arom} (BAR^F₄)), 116.5 (s, CH_{arom}), 76.1 (s, η⁶-C₆H₆), 23.2 (s, py-CH₃).

[(P^rPr)₃(CO)HOS{μ-(κ²-N_{py},N_{imine})₂-BMePI}OsCl(η⁶-C₆H₆)]Cl (11). A solution of 4 (0.070 g, 0.081 mmol) in methanol (5 mL) was treated with [(η⁶-C₆H₆)OsCl₂]₂ (8) (0.027 g, 0.040 mmol) and stirred

for 3 h at room temperature. The volatiles were removed under vacuum, and the residue was washed with diethyl ether (2 × 1 mL) affording a dark red solid. Yield: 0.085 g (87%). A crystal suitable for X-ray diffraction study was obtained from slow diffusion of pentane in a concentrated solution of 11 in dichloromethane (11 contraion was exchanged by BAR^F₄ in order to facilitate the crystallization; the same procedure as the one used for 7). Anal. Calcd. for C₄₅Cl₂H₆₅N₅O₅P₂: C, 44.84; H, 5.44; N, 5.81. Found: C, 45.10; H, 5.51; N, 5.52. HRMS (electrospray, *m/z*): Calcd. for C₄₅ClH₆₅N₅O₅P₂ [M]⁺: 1170.3544, found: 1170.3607. IR (cm^{−1}): ν (CO) 1888 (s). ¹H NMR (400 MHz, CD₂Cl₂, 298 K) δ 8.98 (d, ³J_{H-H} = 7.5, 1H, CH_{arom}), 8.43 (d, ³J_{H-H} = 8.3, 1H, CH_{arom}), 8.29 (d, ³J_{H-H} = 7.5, 1H, CH_{arom}), 7.85–7.74 (m, 3H, CH_{arom}), 7.68 (dd, ³J_{H-H} = 7.5, 7.5, 1H, CH_{arom}), 7.54 (dd, ³J_{H-H} = 7.5, 7.5, 1H, CH_{arom}), 7.16 (d, ³J_{H-H} = 7.7, 1H, CH_{arom}), 7.12 (d, ³J_{H-H} = 7.3, 1H, CH_{arom}), 6.29 (s, 6H, η⁶-C₆H₆), 2.75 (s, 3H, py-CH₃), 2.65 (s, 3H, py-CH₃), 2.43–2.33 (m, 3H, PCH), 2.33–2.22 (m, 3H, PCH), 1.93–0.99 (m, 36H, PCH(CH₃)₂), –14.39 (t, ²J_{H-P} = 20.0, Os-H, 1H). ¹³C{¹H} NMR (100.6 MHz, CD₂Cl₂, 298 K): δ 185.6 (t, ²J_{C-P} = 9.6, CO), 170.7, 169.6, 166.8, 166.0, 158.2, 157.4 (all s, C_{arom}), 140.8 (s, CH_{arom}), 138.7 (s, C_{arom}), 138.2 (s, CH_{arom}), 137.7 (s, C_{arom}), 132.4, 131.0, 125.5, 124.1, 123.3, 121.1, 117.0, 115.3 (all s, CH_{arom}), 76.1 (s, η⁶-C₆H₆), 28.3–27.7 (m, PCH), 25.1 (s, py-CH₃), 23.6 (s, py-CH₃), 20.0 and 19.9 (both s, PCH(CH₃)₂). ³¹P{¹H} NMR (162 MHz, CD₂Cl₂, 298 K): δ 20.5 (AB spin system, Δν = 169.5, ²J_{A-B} = 229.4).

[(P^rPr)₃(CO)HOS{μ-(κ²-N_{py},N_{imine})₂-BMePI}OsCl(η⁶-pCy)]Cl (12). A solution of 4 (0.066 g, 0.076 mmol) in methanol (5 mL) was treated with [(η⁶-p-cymene)OsCl₂]₂ (7) (0.030 g, 0.038 mmol) and stirred for 3 h at room temperature. The volatiles were removed under vacuum, and the residue was washed with diethyl ether (3 × 1.5 mL) affording a reddish-purple solid. Yield: 0.080 g (92%). Anal. Calcd. for C₄₉Cl₂H₇₃N₅O₅P₂: C, 46.66; H, 5.83; N, 5.55. Found: C, 46.85; H, 5.87; N, 5.67. HRMS (electrospray, *m/z*): Calcd. for C₄₉ClH₇₃N₅O₅P₂ [M]⁺: 1226.4171, found: 1226.4235. IR (cm^{−1}): ν (CO) 1897 (s). ¹H NMR (300 MHz, CD₂Cl₂, 298 K) δ 9.06 (d, ³J_{H-H} = 7.5, 1H, CH_{arom}), 8.42 (d, ³J_{H-H} = 8.2, 1H, CH_{arom}), 8.25 (d, ³J_{H-H} = 7.4, 1H, CH_{arom}), 7.86–7.74 (m, 3H, CH_{arom}), 7.68 (dd, ³J_{H-H} = 7.5, 7.4, 1H, CH_{arom}), 7.57 (dd, ³J_{H-H} = 7.5, 7.5, 1H, CH_{arom}), 7.17 (d, ³J_{H-H} = 7.2, 1H, CH_{arom}), 7.15 (d, ³J_{H-H} = 7.2, 1H, CH_{arom}), 6.32 (d, ³J_{H-H} = 5.5, 1H, CH_{arom}(pCy)), 6.01 (d, ³J_{H-H} = 5.6, 1H, CH_{arom}(pCy)), 5.86 (d, ³J_{H-H} = 5.5, 1H, CH_{arom}(pCy)), 5.68 (d, ³J_{H-H} = 5.6, 1H, CH_{arom}(pCy)), 2.71 (s, 3H, py-CH₃), 2.68 (s, 3H, py-CH₃), 2.54 (sept, ³J_{H-H} = 6.9, 1H, pCy-CH(CH₃)₂), 2.43 (s, 3H, CH₃-pCy), 2.42–2.27 (m, 6H, PCH), 1.31 (d, ³J_{H-H} = 6.9, 3H, pCy-CH(CH₃)₂), 1.20–1.04 (m, 36H, PCH(CH₃)₂), 1.20–1.04 (3H, pCy-CH(CH₃)₂, overlapped with PCH(CH₃)₂ signals), –14.50 (t, ²J_{H-P} = 19.9 Os-H, 1H). ¹³C{¹H} NMR (75.5 MHz, CD₂Cl₂, 298 K): δ 185.7 (t, ²J_{C-P} = 9.6, CO), 170.9, 169.5, 166.7, 166.1, 158.4, 157.4 (all s, C_{arom}), 140.9 (s, CH_{arom}), 138.9 (s, C_{arom}), 138.3 (s, CH_{arom}), 137.9 (s, C_{arom}), 132.5, 131.3, 125.7, 124.4, 123.4, 121.3, 117.0, 115.6 (all s, CH_{arom}), 95.9 (s, C_{ipso}(pCy)), 95.2 (s, C_{ipso}(pCy)), 74.1, 73.6, 72.5, 71.3 (both s, CH_{arom}(pCy)), 32.6 (s, pCy-CH(CH₃)₂), 28.2 (vt, N = 17.1, PCH), 28.0 (vt, N = 17.8, PCH), 25.2 (s, py-CH₃), 23.6 (s, py-CH₃), 23.0 (s, pCy-CH(CH₃)₂), 22.6 (s, pCy-CH(CH₃)₂), 20.0 and 20.0 (both s, PCH(CH₃)₂), 19.3 (s, CH₃-pCy). ³¹P{¹H} NMR (121 MHz, CD₂Cl₂, 298 K): δ 20.5 (AB spin system, Δν = 69.0, ²J_{A-B} = 229.1).

General Procedure for the Os-Catalyzed Dehydrogenation Reactions of Alcohols. A solution of the catalyst (0.0178 mmol) and the corresponding substrate (0.254 mmol) in toluene (1 mL) was placed in a Schlenk flask equipped with a condenser. The mixture was stirred at 100 °C for 24 h. After this time the solution was cooled at room temperature, and the progress of the reaction was monitored by GC (Agilent 6890N gas chromatograph with a flame ionization detector, using an Agilent 19091N-133 polyethylene glycol column (30 m × 250 μm × 0.25 μm thickness)). The oven conditions used are as follows: 80 °C (hold 5 min) to 200 °C at 15 °C/min (hold 7 min), except the reaction of dehydrogenation of diphenylmethanol: 150 °C (hold 5 min) to 240 °C at 15 °C/min. For the reactions of dehydrogenation of primary alcohols, yields and molar ratio of

products were determined by ^1H NMR spectroscopy using 1,1,2,2-tetrachloroethane as standard.

General Procedure for the Os-Catalyzed Dehydrogenation Reactions of *N*-Heterocycles and Amines. A solution of the catalyst (0.0119 mmol) and the corresponding substrate (0.119 mmol) in *p*-xylene (1 mL) was placed in a Schlenk flask equipped with a condenser. The mixture was stirred at 140 °C for 48 h. After this time the solution was cooled at room temperature, and the progress of the reaction was monitored by GC (Agilent 6890N gas chromatograph with a flame ionization detector, using an Agilent 19091N-133 polyethylene glycol column (30 m \times 250 μm \times 0.25 μm thickness)) and a Hewlett-Packard 5890 series II gas chromatograph with a flame ionization detector, using a 100% cross-linked methyl silicone gum column (30 m \times 32 mm, with 0.25 μm film thickness). The oven conditions used are as follows: 80 °C (hold 1 min) to 220 °C at 10 °C/min (hold 2 min). For the reactions of dehydrogenation of linear amines, yields and molar ratio of products were determined by ^1H NMR spectroscopy using 1,1,2,2-tetrachloroethane as standard.

Structural Analysis of Complexes 3, 4, 6, 7a, 7b, [9a]Cl, [9b]BAR $^{\text{F}}$ $_4$ and 11. X-ray data were collected for the complexes on a Bruker Smart APEX CCD (3, 6, 7a, 7b, [9b]BAR $^{\text{F}}$ $_4$ and 11) or APEX CCD DUO (4 and [9a]Cl) diffractometer equipped with a 2.4 kW sealed tube source (Mo radiation, $\lambda = 0.71073$ Å) operating at 50 kV and 40 mA (3, 4, 6, 7a, [9b]BAR $^{\text{F}}$ $_4$ and 11) or 30 mA (7b and [9a]Cl). Data were collected over the complete sphere. Each frame exposure time was 10 s (7a, 7b, and [9b]BAR $^{\text{F}}$ $_4$), 20 s (6, [9a]Cl, and 11) or 30 s (3 and 4) covering 0.3° in ω . Data were corrected for absorption by using a multiscan method applied with the SADABS program.³⁹ The structures were solved by Patterson or direct methods and refined by full-matrix least-squares on F^2 with SHELXL97,⁴⁰ including isotropic and subsequently anisotropic displacement parameters. The hydrogen atoms were observed in the least Fourier maps or calculated and refined freely or using a restricted riding model.

The crystal structure of 4 was found to be a nonmerohedral twin of two components. The data were indexed and integrated taking the twinning into account, and the crystal was refined with the reflections file in the HKLF 5 format. The twin law found with the CELL_NOW program is (1.000–0.003 0.002, 0.470–1.001 0.001, 0.476–0.001–0.994). A variable describing the contributions of the two twin components was used in the refinement (BASF instruction). The crystal structure of 7a is also a racemic twin and crystallizes in the noncentrosymmetric *Cc* monoclinic space group with a Flack parameter of ≈ 0.5 .

In 6 two isopropyl groups of a phosphine ligand were observed disordered and refined with different moieties, complementary occupancy factors, restrained geometry, and isotropic displacement parameters.

In 7a, only one dimer is found in the asymmetric unit, but the BF $_4$ anion, dichloromethane of crystallization, and a phosphine ligand were found disordered and refined in the same way as 6, while in 7b only the dichloromethane of crystallization was found disordered.

11 crystallizes with two dimers in the asymmetric unit. In both molecules the benzene ligands were observed disordered, along with several CF $_3$ groups of the BAR $^{\text{F}}$ $_4$ anions and dichloromethane of crystallization. The refinement was performed in a similar way to 6. In [9a]Cl (solvent) and [9b]BAR $^{\text{F}}$ $_4$ (anion) the same problems were encountered and refined in the same way.

Crystal Data for 3. C $_{38}\text{H}_{61}\text{N}_5\text{OsP}_2$, M_{W} 840.05, red, irregular block (0.161 \times 0.110 \times 0.017), monoclinic, space group $P2_1/c$, a : 15.315(4) Å, b : 16.276(4) Å, c : 15.480(4) Å, β : 98.653(3)°, $V = 3814.7(16)$ Å 3 , $Z = 4$, $Z' = 1$, D_{calc} : 1.463 g cm $^{-3}$, $F(000)$: 1720, $T = 100(2)$ K, μ 3.460 mm $^{-1}$. 26981 measured reflections (2θ : 3–57°, ω scans 0.3°), 6785 unique ($R_{\text{int}} = 0.1167$); min./max. transm. Factors 0.572/0.862. Final agreement factors were $R^1 = 0.0527$ (4474 observed reflections, $I > 2\sigma(I)$) and $wR^2 = 0.1268$; data/restraints/parameters 6785/17/439; GoF = 0.991. Largest peak and hole: 2.453 (close to osmium atoms) and -2.519 e/ Å 3 .

Crystal Data for 4. C $_{39}\text{H}_{59}\text{N}_5\text{OOSp}_2$, CH $_4\text{O}$, M_{W} 898.09, orange, irregular block (0.36 \times 0.12 \times 0.06), triclinic, space group $P-1$, a : 15.189(3) Å, b : 16.201(3) Å, c : 18.352(4) Å, α : 68.87(3)°, β :

78.85(3)°, γ : 77.29(3)°, $V = 4076.8(17)$ Å 3 , $Z = 4$, $Z' = 2$, D_{calc} : 1.463 g cm $^{-3}$, $F(000)$: 1840, $T = 100(2)$ K, μ 3.246 mm $^{-1}$. 43865 measured reflections (2θ : 3–58°, ω scans 0.3°), 30923 unique ($R_{\text{int}} = 0.0485$); min./max. transm. Factors 0.575/0.862. Final agreement factors were $R^1 = 0.0372$ (22654 observed reflections, $I > 2\sigma(I)$) and $wR^2 = 0.0879$; data/restraints/parameters 30923/2/940; GoF = 1.025. Largest peak and hole: 4.158 (close to osmium atom) and -2.666 e/ Å 3 .

Crystal Data for 6. C $_{56}\text{H}_{106}\text{N}_5\text{Os}_2\text{P}_4$, C $_{22}\text{H}_{30}\text{O}_2\text{S}$, Cl, M_{W} 1747.70, violet, irregular block (0.231 \times 0.071 \times 0.066), monoclinic, space group $P2_1/n$, a : 10.3148(6) Å, b : 21.0494(12) Å, c : 38.045(2) Å, β : 95.6450(10)°, $V = 8220.3(8)$ Å 3 , $Z = 4$, $Z' = 1$, D_{calc} : 1.412 g cm $^{-3}$, $F(000)$: 3600, $T = 100(2)$ K, μ 3.270 mm $^{-1}$. 81497 measured reflections (2θ : 3–57°, ω scans 0.3°), 19737 unique ($R_{\text{int}} = 0.0705$); min./max. transm. Factors 0.667/0.862. Final agreement factors were $R^1 = 0.0491$ (14612 observed reflections, $I > 2\sigma(I)$) and $wR^2 = 0.0924$; data/restraints/parameters 19737/22/882; GoF = 1.060. Largest peak and hole: 1.730 (close to osmium atoms) and -1.498 e/ Å 3 .

Crystal Data for 7a. C $_{58}\text{H}_{102}\text{N}_5\text{O}_2\text{Os}_2\text{P}_4$, BF $_4$, 1.5(CH $_2\text{Cl}_2$), M_{W} 1619.93, red, irregular block (0.19 \times 0.02 \times 0.02), monoclinic, space group Cc , a : 27.998(2) Å, b : 18.5935(16) Å, c : 19.606(3) Å, β : 131.4400(10)°, $V = 7651.5(15)$ Å 3 , $Z = 4$, $Z' = 1$, D_{calc} : 1.406 g cm $^{-3}$, $F(000)$: 3268, $T = 100(2)$ K, μ 3.555 mm $^{-1}$. 33890 measured reflections (2θ : 3–57°, ω scans 0.3°), 17194 unique ($R_{\text{int}} = 0.0460$); min./max. transm. Factors 0.584/0.862. Final agreement factors were $R^1 = 0.0625$ (14359 observed reflections, $I > 2\sigma(I)$) and $wR^2 = 0.1635$; Flack parameter: 0.52(1); data/restraints/parameters 17194/111/738; GoF = 1.036. Largest peak and hole: 2.234 (close to osmium atoms) and -2.009 e/ Å 3 .

Crystal Data for 7b. C $_{58}\text{H}_{102}\text{N}_5\text{O}_2\text{Os}_2\text{P}_4$, BF $_4$, 2.5(CH $_2\text{Cl}_2$), M_{W} 1704.85, red, irregular block (0.15 \times 0.15 \times 0.10), triclinic, space group $P-1$, a : 10.7229(5) Å, b : 17.5586(7) Å, c : 19.5024(8) Å, α : 96.5720(10)°, β : 93.1670(10)°, γ : 93.9360(10)°, $V = 3631.8(3)$ Å 3 , $Z = 2$, $Z' = 1$, D_{calc} : 1.559 g cm $^{-3}$, $F(000)$: 1718, $T = 100(2)$ K, μ 3.820 mm $^{-1}$. 44350 measured reflections (2θ : 3–57°, ω scans 0.3°), 16899 unique ($R_{\text{int}} = 0.0738$); min./max. transm. Factors 0.687/0.862. Final agreement factors were $R^1 = 0.0380$ (13252 observed reflections, $I > 2\sigma(I)$) and $wR^2 = 0.0928$; data/restraints/parameters 16899/6/780; GoF = 0.998. Largest peak and hole: 1.676 (close to osmium atoms) and -1.808 e/ Å 3 .

Crystal Data for [9a]Cl. C $_{32}\text{H}_{28}\text{Cl}_2\text{N}_5\text{Os}_2$, Cl, 3.65(CH $_2\text{Cl}_2$), M_{W} 1279.32, red, irregular block (0.14 \times 0.06 \times 0.02), triclinic, space group $P-1$, a : 10.8057(17) Å, b : 11.3263(18) Å, c : 18.215(3) Å, α : 91.548(2)°, β : 106.232(2)°, γ : 99.684(2)°, $V = 2103.5(6)$ Å 3 , $Z = 2$, $Z' = 1$, D_{calc} : 2.020 g cm $^{-3}$, $F(000)$: 1223, $T = 100(2)$ K, μ 6.724 mm $^{-1}$. 22743 measured reflections (2θ : 3–57°, ω scans 0.3°), 10545 unique ($R_{\text{int}} = 0.0338$); min./max. transm. Factors 0.575/0.862. Final agreement factors were $R^1 = 0.0348$ (8234 observed reflections, $I > 2\sigma(I)$) and $wR^2 = 0.0868$; data/restraints/parameters 10545/8/486; GoF = 1.022. Largest peak and hole: 2.258 (close to osmium atoms) and -2.498 e/ Å 3 .

Crystal Data for [9b]BAR $^{\text{F}}$ $_4$. C $_{32}\text{H}_{28}\text{Cl}_2\text{N}_5\text{Os}_2$, C $_{32}\text{H}_{12}\text{BF}_4$, 2-(CH $_2\text{Cl}_2$), M_{W} 1966.97, orange, irregular block (0.16 \times 0.07 \times 0.07), monoclinic, space group $P2_1/c$, a : 11.9316(6) Å, b : 27.9130(14) Å, c : 20.8299(11) Å, β : 99.4040(10)°, $V = 6844.1(6)$ Å 3 , $Z = 4$, $Z' = 1$, D_{calc} : 1.909 g cm $^{-3}$, $F(000)$: 3800, $T = 100(2)$ K, μ 4.056 mm $^{-1}$. 48364 measured reflections (2θ : 3–57°, ω scans 0.3°), 16171 unique ($R_{\text{int}} = 0.0568$); min./max. transm. Factors 0.680/0.862. Final agreement factors were $R^1 = 0.0476$ (11998 observed reflections, $I > 2\sigma(I)$) and $wR^2 = 0.0884$; data/restraints/parameters 16171/61/917; GoF = 1.052. Largest peak and hole 1.726 (close to osmium atoms) and -1.739 e/ Å 3 .

Crystal Data for 11. C $_{45}\text{H}_{65}\text{ClN}_5\text{OOSp}_2$, C $_{32}\text{H}_{12}\text{BF}_4$, 1.975-(CH $_2\text{Cl}_2$), 0.125 (C $_5\text{H}_{12}$), M_{W} 2209.78, orange, irregular block (0.26 \times 0.23 \times 0.09), triclinic, space group $P-1$, a : 12.6210(12) Å, b : 25.864(2) Å, c : 28.215(3) Å, α : 87.3890(10)°, β : 82.1900(10)°, γ : 82.8930(10)°, $V = 9050.9(15)$ Å 3 , $Z = 4$, $Z' = 2$, D_{calc} : 1.622 g cm $^{-3}$, $F(000)$: 4361, $T = 100(2)$ K, μ 3.081 mm $^{-1}$. 109359 measured reflections (2θ : 3–57°, ω scans 0.3°), 41929 unique ($R_{\text{int}} = 0.0449$); min./max. transm. Factors 0.661/0.862. Final agreement factors were $R^1 = 0.0747$ (31471 observed reflections, $I > 2\sigma(I)$) and $wR^2 = 0.1815$; data/restraints/

parameters 41929/213/2029; GoF = 1.123. Largest peak and hole: 3.558 (close to osmium atoms) and $-2.205 \text{ e}/\text{\AA}^3$.

■ ASSOCIATED CONTENT

■ Supporting Information

The Supporting Information is available free of charge on the ACS Publications website at DOI: [10.1021/acs.organomet.7b00906](https://doi.org/10.1021/acs.organomet.7b00906).

UV–vis spectra, redox studies, computational details, NMR spectra of complexes **3**, **4**, **6**, **7**, **9a**, **9b**, **11**, and **12** (PDF)

Cartesian coordinates of computed complexes (XYZ)

Accession Codes

CCDC [1812164](https://doi.org/10.1107/CCDC1812164)–[1812171](https://doi.org/10.1107/CCDC1812171) (**3**, **7a**, **4**, **7b**, **6**, [**9a**]**Cl**, [**9b**]**BAr^F₄**, **11**) contain the supplementary crystallographic data for this paper. These data can be obtained free of charge via www.ccdc.cam.ac.uk/data_request/cif, or by emailing data_request@ccdc.cam.ac.uk, or by contacting The Cambridge Crystallographic Data Centre, 12 Union Road, Cambridge CB2 1EZ, UK; fax: +44 1223 336033.

■ AUTHOR INFORMATION

Corresponding Authors

*E-mail: maester@unizar.es.

*E-mail: sierraor@ucm.es.

ORCID

Miguel A. Esteruelas: 0000-0002-4829-7590

M. Pilar Gay: 0000-0001-8056-1083

Mar Gómez-Gallego: 0000-0002-8961-7685

Enrique Oñate: 0000-0003-2094-719X

Alicia Santiago: 0000-0003-0614-2491

Miguel A. Sierra: 0000-0002-3360-7795

Notes

The authors declare no competing financial interest.

■ ACKNOWLEDGMENTS

Financial support from the Spanish Ministerio de Economía y Competitividad (MINECO) (Projects CTQ2017-82935-P, Red de Excelencia Consolider CTQ2016-81797-REDC), the Gobierno de Aragón (E35), Fondo Europeo de Desarrollo Regional (FEDER), and the European Social Fund (FSE) is acknowledged.

■ REFERENCES

- (1) (a) Friedrich, A.; Schneider, S. *ChemCatChem* **2009**, *1*, 72–73. (b) Trincado, M.; Banerjee, D.; Grützmacher, H. *Energy Environ. Sci.* **2014**, *7*, 2464–2503. (c) Werkmeister, S.; Neumann, J.; Junge, K.; Beller, M. *Chem. - Eur. J.* **2015**, *21*, 12226–12250. (d) Nielsen, M. *Hydrogen Pollution and Remediation Carbon and Pollutants*; Lichtfouse, E., Schwarzbauer, J., Robert, D., Eds.; Springer International Publishing: Switzerland, 2015; Chapter 1, pp 2–6, DOI: [10.1007/978-3-319-19375-5](https://doi.org/10.1007/978-3-319-19375-5). (e) Crabtree, R. H. *Chem. Rev.* **2017**, *117*, 9228–9246.
- (2) (a) Crabtree, R. H. *Energy Environ. Sci.* **2008**, *1*, 134. (b) Giustra, Z. X.; Ishibashi, J. S. A.; Liu, S.-Y. *Coord. Chem. Rev.* **2016**, *314*, 134–181. (c) Preuster, P.; Papp, C.; Wasserscheid, P. *Acc. Chem. Res.* **2017**, *50*, 74–85.
- (3) For dehydrogenation of alcohols, see: (a) Murahashi, S. I.; Naota, T.; Ito, K.; Maeda, Y.; Taki, H. *J. Org. Chem.* **1987**, *52*, 4319–4327. (b) Zhao, J.; Hartwig, J. F. *Organometallics* **2005**, *24*, 2441–2446. (c) Prades, A.; Peris, E.; Albrecht, M. *Organometallics* **2011**, *30*, 1162–1167. (d) Buntara, T.; Noel, S.; Phua, P. H.; Melián-Cabrera, I.; De Vries, J. G.; Heeres, H. J. *Angew. Chem., Int. Ed.* **2011**, *50*, 7083–7087.

- (e) Nielsen, M.; Kammer, A.; Cozzula, D.; Junge, H.; Gladiali, S.; Beller, M. *Angew. Chem., Int. Ed.* **2011**, *50*, 9593–9597. (f) Zhang, J.; Balaraman, E.; Leitens, G.; Milstein, D. *Organometallics* **2011**, *30*, 5716–5724. (g) Muthaiah, S.; Hong, S. H. *Adv. Synth. Catal.* **2012**, *354*, 3045–3053. (h) Tseng, K.-N. T.; Kampf, J. W.; Szymczak, N. K. *Organometallics* **2013**, *32*, 2046–2049. (i) Langer, R.; Fuchs, I.; Vogt, M.; Balaraman, E.; Diskin-Posner, Y.; Shimon, L. J. W.; Ben-David, Y.; Milstein, D. *Chem. - Eur. J.* **2013**, *19*, 3407–3414. (j) Tseng, K.-N. T.; Kampf, J. W.; Szymczak, N. K. *ACS Catal.* **2015**, *5*, 5468–5485. (k) Dutta, I.; Sarbajna, A.; Pandey, P.; Rahaman, S. M. W.; Singh, K.; Bera, J. K. *Organometallics* **2016**, *35*, 1505–1513. (l) Wang, Z.; Pan, B.; Liu, Q.; Yue, E.; Solan, G. A.; Ma, Y.; Sun, W.-H. *Catal. Sci. Technol.* **2017**, *7*, 1654–1661. (m) Sarbajna, A.; Dutta, I.; Daw, P.; Dinda, S.; Rahaman, S. M. W.; Sarkar, A.; Bera, J. K. *ACS Catal.* **2017**, *7*, 2786–2790. (n) De Boer, S. Y.; Korstanje, T. J.; La Rooij, S. R.; Kox, R.; Reek, J. N. H.; Van Der Lugt, J. I. *Organometallics* **2017**, *36*, 1541–1549. (o) Wang, Q.; Chai, H.; Yu, Z. *Organometallics* **2017**, *36*, 3638–3644. (p) Pretorius, R.; Olguín, J.; Albrecht, M. *Inorg. Chem.* **2017**, *56*, 12410–12420.
- (4) For dehydrogenation of cyclic amines, see: Tsuji, Y.; Kotachi, S.; Huh, K. T.; Watanabe, Y. *J. Org. Chem.* **1990**, *55*, 580–584.
- (5) For dehydrogenation of alcohols, see: (a) Toyomura, K.; Fujita, K. *Chem. Lett.* **2017**, *46*, 808–810. (b) Yamaguchi, R.; Kobayashi, D.; Shimizu, M.; Fujita, K. *J. Organomet. Chem.* **2017**, *843*, 14–19. (c) Fujita, K.; Tamura, R.; Tanaka, Y.; Yoshida, M.; Onoda, M.; Yamaguchi, R. *ACS Catal.* **2017**, *7*, 7226–7230. (d) Mazloomi, Z.; Pretorius, R.; Pàmies, O.; Albrecht, M.; Diéguez, M. *Inorg. Chem.* **2017**, *56*, 11282–11298. (e) González Miera, G.; Martínez-Castro, E.; Martín-Matute, B. *Organometallics* **2017**, DOI: [10.1021/acs.organomet.7b00220](https://doi.org/10.1021/acs.organomet.7b00220).
- (6) For dehydrogenation of cyclic amines, see: (a) Wang, Z.; Tonks, I.; Belli, J.; Jensen, C. M. *J. Organomet. Chem.* **2009**, *694*, 2854–2857. (b) Yamaguchi, R.; Ikeda, C.; Takahashi, Y.; Fujita, K. *J. Am. Chem. Soc.* **2009**, *131*, 8410–8412. (c) Zhang, X.-B.; Xi, Z. *Phys. Chem. Chem. Phys.* **2011**, *13*, 3997. (d) Li, H.; Jiang, J.; Lu, G.; Huang, F.; Wang, Z. X. *Organometallics* **2011**, *30*, 3131–3141. (e) Wu, J.; Talwar, D.; Johnston, S.; Yan, M.; Xiao, J. *Angew. Chem., Int. Ed.* **2013**, *52*, 6983–6987. (f) Fujita, K.; Tanaka, Y.; Kobayashi, M.; Yamaguchi, R. *J. Am. Chem. Soc.* **2014**, *136*, 4829–4832. (g) Talwar, D.; Gonzalez-de-Castro, A.; Li, H. Y.; Xiao, J. *Angew. Chem., Int. Ed.* **2015**, *54*, 5223–5227. (h) Kojima, M.; Kanai, M. *Angew. Chem., Int. Ed.* **2016**, *55*, 12224–12227. (i) Fujita, K.-I.; Wada, T.; Shiraishi, T. *Angew. Chem., Int. Ed.* **2017**, *56*, 10886–10889.
- (7) For dehydrogenation of alcohols, see: (a) Song, H.; Kang, B.; Hong, S. H. *ACS Catal.* **2014**, *4*, 2889–2895. (b) Chakraborty, S.; Lagaditis, P. O.; Förster, M.; Bielinski, E. A.; Hazari, N.; Holthausen, M. C.; Jones, W. D.; Schneider, S. *ACS Catal.* **2014**, *4*, 3994–4003. (c) Kamitani, M.; Ito, M.; Itazaki, M.; Nakazawa, H. *Chem. Commun.* **2014**, *50*, 7941–7944. (d) Bonitatibus, P. J.; Chakraborty, S.; Doherty, M. D.; Siclován, O.; Jones, W. D.; Soloveichik, G. L. *Proc. Natl. Acad. Sci. U. S. A.* **2015**, *112*, 1687–1692. (e) Chakraborty, S.; Pizsel, P. E.; Brennessel, W. W.; Jones, W. D. *Organometallics* **2015**, *34*, 5203–5206. (f) Dai, Z.; Luo, Q.; Jiang, H.; Luo, Q.; Li, H.; Zhang, J.; Peng, T. *Catal. Sci. Technol.* **2017**, *7*, 2506–2511.
- (8) For dehydrogenation of cyclic amines, see: (a) Mikami, Y.; Ebata, K.; Mitsudome, T.; Mizugaki, T.; Jitsukawa, K.; Kaneda, K. *Heterocycles* **2011**, *82*, 1371–1377. (b) Luca, O. R.; Huang, D. L.; Takase, M. K.; Crabtree, R. H. *New J. Chem.* **2013**, *37*, 3402–3405. (c) Chakraborty, S.; Brennessel, W. W.; Jones, W. D. *J. Am. Chem. Soc.* **2014**, *136*, 8564–8567. (d) Xu, R.; Chakraborty, S.; Yuan, H.; Jones, W. D. *ACS Catal.* **2015**, *5*, 6350–6354. (e) Ventura-Espinosa, D.; Marzá-Beltrán, A.; Mata, J. A. *Chem. - Eur. J.* **2016**, *22*, 17758–17766. (f) Zhou, W.; Taboonpong, P.; Aboo, A. H.; Zhang, L.; Jiang, J.; Xiao, J. *Synlett* **2016**, *27*, 1806–1809. (g) Sawatlon, B.; Surawatanawong, P. *Dalton Trans.* **2016**, *45*, 14965–14978.
- (9) (a) Sauer, D. C.; Melen, R. L.; Kruck, M.; Gade, L. H. *Eur. J. Inorg. Chem.* **2014**, *2014*, 4715–4725. (b) Csonka, R.; Speier, G.; Kaizer, J. *RSC Adv.* **2015**, *5*, 18401–18419.

- (10) Müller, A. L.; Bleith, T.; Roth, T.; Wadepohl, H.; Gade, L. H. *Organometallics* **2015**, *34*, 2326–2342.
- (11) (a) Baird, D. M.; Hassan, R.; Kim, W. K. *Inorg. Chim. Acta* **1987**, *130*, 39–42. (b) Baird, D. M.; Shih, K. Y. *Polyhedron* **1989**, *8*, 2359–2365. (c) Baird, D. M.; Shih, K. Y. *Polyhedron* **1991**, *10*, 229–235.
- (12) (a) Gagné, R. R.; Marritt, W. A.; Marks, D. N.; Siegl, W. O. *Inorg. Chem.* **1981**, *20*, 3260–3267. (b) Anderson, O. P.; La Cour, A.; Dodd, A.; Garrett, A. D.; Wicholas, M. *Inorg. Chem.* **2003**, *42*, 122–127. (c) Wicholas, M.; Garrett, A. D.; Gleaves, M.; Morris, A. M.; Rehm, M.; Anderson, O. P.; La Cour, A. *Inorg. Chem.* **2006**, *45*, 5804–5811. (d) Pap, J. S.; Kripli, B.; Giorgi, M.; Kaizer, J.; Speier, G. *Transition Met. Chem.* **2011**, *36*, 481–487. (e) Sauer, D. C.; Wadepohl, H. *Polyhedron* **2014**, *33*, 180–187. (f) Zhang, D. B.; Wang, J. Y.; Wen, H.-M.; Chen, Z.-N. *Organometallics* **2014**, *33*, 4738–4746. (g) Roth, T.; Wadepohl, H.; Gade, L. H. *Eur. J. Inorg. Chem.* **2016**, *2016*, 1184–1191.
- (13) (a) Kolb, H. C.; VanNieuwenhze, M. S.; Sharpless, K. B. *Chem. Rev.* **1994**, *94*, 2483–2547. (b) Döbler, C.; Mehlretter, G. M.; Sundermeier, U.; Beller, M. *J. Am. Chem. Soc.* **2000**, *122*, 10289–10297. (c) Döbler, C.; Mehlretter, G. M.; Sundermeier, U.; Beller, M. *J. Organomet. Chem.* **2001**, *621*, 70–76. (d) Heravi, M. M.; Zadsirjan, V.; Esfandyari, M.; Lashaki, T. B. *Tetrahedron: Asymmetry* **2017**, *28*, 987–1043.
- (14) See for example: (a) Esteruelas, M. A.; Honczek, N.; Oliván, M.; Oñate, E.; Valencia, M. *Organometallics* **2011**, *30*, 2468–2471. (b) Bertoli, M.; Choualeb, A.; Lough, A. J.; Moore, B.; Spasyuk, D.; Gusev, D. G. *Organometallics* **2011**, *30*, 3479–3482. (c) Buil, M. L.; Esteruelas, M. A.; Herrero, J.; Izquierdo, S.; Pastor, I. M.; Yus, M. *ACS Catal.* **2013**, *3*, 2072–2075. (d) Esteruelas, M. A.; Fernández, I.; López, A. M.; Mora, M.; Oñate, E. *Organometallics* **2014**, *33*, 1104–1107. (e) Spasyuk, D.; Vicent, C.; Gusev, D. G. *J. Am. Chem. Soc.* **2015**, *137*, 3743–3746. (f) Chelucci, G.; Baldino, S.; Baratta, W. *Acc. Chem. Res.* **2015**, *48*, 363–379. (g) Esteruelas, M. A.; López, A. M.; Mora, M.; Oñate, E. *ACS Catal.* **2015**, *5*, 187–191. (h) Bolaño, T.; Esteruelas, M. A.; Gay, M. P.; Oñate, E.; Pastor, I. M.; Yus, M. *Organometallics* **2015**, *34*, 3902–3908.
- (15) (a) Baratta, W.; Bossi, G.; Putignano, E.; Rigo, P. *Chem. - Eur. J.* **2011**, *17*, 3474–3481. (b) Chelucci, G.; Baldino, S.; Baratta, W. *Coord. Chem. Rev.* **2015**, *300*, 29–85.
- (16) Esteruelas, M. A.; Lezáun, V.; Martínez, A.; Oliván, M.; Oñate, E. *Organometallics* **2017**, *36*, 2996–3004.
- (17) Bröring, M.; Kleeberg, C. J. *Porphyrins Phthalocyanines* **2008**, *12*, 839–844.
- (18) Dietrich, B. L.; Egbert, J.; Morris, A. M.; Wicholas, M.; Anderson, O. P.; Miller, S. M. *Inorg. Chem.* **2005**, *44*, 6476–6481.
- (19) (a) Esteruelas, M. A.; Fernández-Álvarez, F. J.; Oñate, E. *J. Am. Chem. Soc.* **2006**, *128*, 13044–13045. (b) Álvarez, E.; Conejero, S.; Paneque, M.; Petronilho, A.; Poveda, M. L.; Serrano, O.; Carmona, E. *J. Am. Chem. Soc.* **2006**, *128*, 13060–13061. (c) Álvarez, E.; Conejero, S.; Lara, P.; López, J. A.; Paneque, M.; Petronilho, A.; Poveda, M. L.; Del Río, D.; Serrano, O.; Carmona, E. *J. Am. Chem. Soc.* **2007**, *129*, 14130–14131. (d) Buil, M. L.; Esteruelas, M. A.; Garcés, K.; Oliván, M.; Oñate, E. *J. Am. Chem. Soc.* **2007**, *129*, 10998–10999. (e) Esteruelas, M. A.; Fernández-Álvarez, F. J.; Oñate, E. *Organometallics* **2007**, *26*, 5239–5245. (f) Buil, M. L.; Esteruelas, M. A.; Garcés, K.; Oliván, M.; Oñate, E. *Organometallics* **2008**, *27*, 4680–4690. (g) Conejero, S.; Lara, P.; Paneque, M.; Petronilho, A.; Poveda, M. L.; Serrano, O.; Vattier, F.; Álvarez, E.; Maya, C.; Salazar, V.; Carmona, E. *Angew. Chem., Int. Ed.* **2008**, *47*, 4380–4383. (h) Esteruelas, M. A.; Fernández-Álvarez, F. J.; Oliván, M.; Oñate, E. *Organometallics* **2009**, *28*, 2276–2284. (i) Paneque, M.; Poveda, M. L.; Vattier, F.; Álvarez, E.; Carmona, E. *Chem. Commun.* **2009**, 5561–5563. (j) Su, Y.; Song, G.; Han, K.; Li, X. *J. Organomet. Chem.* **2011**, *696*, 1640–1646. (k) Bajo, S.; Esteruelas, M. A.; López, A. M.; Oñate, E. *Organometallics* **2012**, *31*, 8618–8626. (l) Conejero, S.; Maya, C.; Paneque, M.; Petronilho, A.; Poveda, M. L.; Vattier, F.; Álvarez, E.; Carmona, E.; Laguna, A.; Crespo, O. *Dalton Trans.* **2012**, *41*, 14126. (m) Bajo, S.; Esteruelas, M. A.; López, A. M.; Oñate, E. *Organometallics* **2014**, *33*, 1851–1858. (n) Bajo, S.; Esteruelas, M. A.; López, A. M.; Oñate, E. *Organometallics* **2014**, *33*, 4057–4066.
- (20) Esteruelas, M. A.; López, A. M.; Oliván, M. *Chem. Rev.* **2016**, *116*, 8770–8847.
- (21) (a) Esteruelas, M. A.; Masamunt, A. B.; Oliván, M.; Oñate, E.; Valencia, M. *J. Am. Chem. Soc.* **2008**, *130*, 11612–11613. (b) Esteruelas, M. A.; Fernández, I.; Herrera, A.; Martín-Ortiz, M.; Martínez-Álvarez, R.; Oliván, M.; Oñate, E.; Sierra, M. A.; Valencia, M. *Organometallics* **2010**, *29*, 976–986. (c) Crespo, O.; Eguillor, B.; Esteruelas, M. A.; Fernández, I.; García-Raboso, J.; Gómez-Gallego, M.; Martín-Ortiz, M.; Oliván, M.; Sierra, M. A. *Chem. Commun.* **2012**, *48*, 5328. (d) Alabau, R. G.; Eguillor, B.; Esler, J.; Esteruelas, M. A.; Oliván, M.; Oñate, E.; Tsai, J.-Y.; Xia, C. *Organometallics* **2014**, *33*, 5582–5596. (e) Esteruelas, M. A.; Larramona, C.; Oñate, E. *Organometallics* **2016**, *35*, 1597–1600. (f) Eguillor, B.; Esteruelas, M. A.; Lezáun, V.; Oliván, M.; Oñate, E.; Tsai, J.-Y.; Xia, C. *Chem. - Eur. J.* **2016**, *22*, 9106–9110. (g) Eguillor, B.; Esteruelas, M. A.; Lezáun, V.; Oliván, M.; Oñate, E. *Chem. - Eur. J.* **2017**, *23*, 1526–1530.
- (22) (a) Casarrubios, L.; Esteruelas, M. A.; Larramona, C.; Lledós, A.; Muntaner, J. G.; Oñate, E.; Ortuño, M. A.; Sierra, M. A. *Chem. - Eur. J.* **2015**, *21*, 16781–16785. (b) Casarrubios, L.; Esteruelas, M. A.; Larramona, C.; Muntaner, J. G.; Oñate, E.; Sierra, M. A. *Inorg. Chem.* **2015**, *54*, 10998–11006.
- (23) Esteruelas, M. A.; García-Raboso, J.; Oliván, M.; Oñate, E. *Inorg. Chem.* **2012**, *51*, 5975–5984.
- (24) (a) Eguillor, B.; Esteruelas, M. A.; García-Raboso, J.; Oliván, M.; Oñate, E.; Pastor, I. M.; Peñafiel, I.; Yus, M. *Organometallics* **2011**, *30*, 1658–1667. (b) Esteruelas, M. A.; García-Raboso, J.; Oliván, M. *Organometallics* **2011**, *30*, 3844–3852.
- (25) (a) Casarrubios, L.; Esteruelas, M. A.; Larramona, C.; Muntaner, J. G.; Oliván, M.; Oñate, E.; Sierra, M. A. *Organometallics* **2014**, *33*, 1820–1833. (b) Eguillor, B.; Esteruelas, M. A.; Fernández, I.; Gómez-Gallego, M.; Lledós, A.; Martín-Ortiz, M.; Oliván, M.; Oñate, E.; Sierra, M. A. *Organometallics* **2015**, *34*, 1898–1910. (c) Alabau, R. G.; Esteruelas, M. A.; Oliván, M.; Oñate, E. *Organometallics* **2017**, *36*, 1848–1859.
- (26) Müller, A. L.; Wadepohl, H.; Gade, L. H. *Organometallics* **2015**, *34*, 2810–2818.
- (27) Adwood, J. D. *Inorganic and Organometallic Reaction Mechanisms*; VCH Publishers: New York, 1997; Chapter 3.
- (28) The alcohol is the source of the third hydride ligand of each $\text{OsH}_3(\text{P}^i\text{Pr}_3)_2$ moiety.
- (29) Crabtree, R. H. *Chem. Rev.* **2016**, *116*, 8750–8769.
- (30) This species was generated *in situ* according to a previously described procedure. See: Batuecas, M.; Castro-Rodrigo, R.; Esteruelas, M. A.; García-Yebra, C.; López, A. M.; Oñate, E. *Angew. Chem., Int. Ed.* **2016**, *55*, 13749–13753.
- (31) Aracama, M.; Esteruelas, M. A.; Lahoz, F. J.; López, J. A.; Meyer, U.; Oro, L. A.; Werner, H. *Inorg. Chem.* **1991**, *30*, 288–293.
- (32) Edwards, A. J.; Elipe, S.; Esteruelas, M. A.; Lahoz, F. J.; Oro, L. A.; Valero, C. *Organometallics* **1997**, *16*, 3828–3836.
- (33) Esteruelas, M. A.; Werner, H. *J. Organomet. Chem.* **1986**, *303*, 221–231.
- (34) Castarlenas, R.; Esteruelas, M. A.; Oñate, E. *Organometallics* **2005**, *24*, 4343–4346.
- (35) Arthur, T.; Stephenson, T. A. *J. Organomet. Chem.* **1981**, *208*, 369–387.
- (36) Siegl, W. O. *J. Org. Chem.* **1977**, *42*, 1872–1878.
- (37) Funk, J. K.; Yennawar, H.; Sen, A. *Helv. Chim. Acta* **2006**, *89*, 1687–1695.
- (38) Iinuma, M.; Moriyama, K.; Togo, H. *Tetrahedron* **2013**, *69*, 2961–2970.
- (39) Blessing, R. H. *Acta Crystallogr., Sect. A: Found. Crystallogr.* **1995**, *51*, 33–38. SADABS: Area-detector absorption correction; Bruker-AXS: Madison, WI, 1996.
- (40) Sheldrick, G. M. *Acta Crystallogr., Sect. A: Found. Crystallogr.* **2008**, *64*, 112–122.